

SPACE PHOTOMETRY WITH BRITE-CONSTELLATION*

Werner W. Weiss^{1,†,*}, Konstanze Zwintz², Rainer Kuschnig³, Gerald Handler⁴, Anthony F. J. Moffat⁵, Dietrich Baade⁶, Dominic M. Bowman⁷, Thomas Granzer⁸, Thomas Kallinger⁹, Otto F. Koudelka¹⁰, Catherine C. Lovekin¹¹, Coralie Neiner¹², Herbert Pablo¹³, Andrzej Pigulski¹⁴, Adam Popowicz¹⁵, Tahina Ramiaramanantsoa¹⁶, Slavek M. Rucinski¹⁷, Klaus G. Strassmeier¹⁸, Gregg A. Wade¹⁹

¹werner.weiss@univie.ac.at, ²konstanze.zwintz@uibk.ac.at, ³rainer.kuschnig@tugraz.at, ⁴gerald@camk.edu.pl, ⁵amoffat@sympatico.ca, ⁶dbaade@eso.org, ⁷dominic.bowman@kuleuven.be, ⁸tgranzer@aip.de, ⁹kallinger@astro.univie.ac.at, ¹⁰koudelka@TU Graz.at, ¹¹clovekin@mta.ca, ¹²coralie.neiner@obspm.fr, ¹³hpablo@aaavso.org, ¹⁴pigulski@astro.uni.wroc.pl, ¹⁵Adam.Popowicz@polsl.pl, ¹⁶tahina@asu.edu, ¹⁷rucinski@astro.utoronto.ca, ¹⁸kstrassmeier@aip.de, ¹⁹Gregg.Wade@rmc.ca

* Correspondence: werner.weiss@univie.ac.at

† Current address: University of Vienna, Department of Astrophysics, Tuerkenschanzstrasse 17, Vienna, Austria

Abstract: BRITE-CONSTELLATION is devoted to high-precision optical photometric monitoring of bright stars, distributed all over the Milky Way, in red and/or blue passbands. Photometry from space avoids the turbulent and absorbing terrestrial atmosphere and allows for very long and continuous observing runs with high time resolution and thus provides the data necessary for understanding various processes inside stars (e.g. asteroseismology) and in their immediate environment. While the first astronomical observations from space focused on the spectral regions not accessible from ground it soon became obvious around 1970 that avoiding the turbulent terrestrial atmosphere improved significantly the accuracy of photometry and satellites explicitly dedicated to high-quality photometry were launched. A perfect example is BRITE-CONSTELLATION, which is the result of a very successful cooperation of Austria, Canada and Poland. Research highlights for targets distributed nearly over the entire HRD are presented, but focus primarily on massive and hot stars.

Citation: Weiss W., Zwintz K., Kuschnig R., Handler G., Moffat A., Baade D., et al.: Space Photometry with BRITE-CONSTELLATION. *Universe* **2021**, *1*, 0.
<https://dx.doi.org/>

Keywords: Space photometry; Stellar structure; Stellar evolution; Stellar environment; Nanosatellites

Received: tbd

Accepted:

Published:

Publisher's Note: MDPI stays neutral with regard to jurisdictional claims in published maps and institutional affiliations.

Copyright: © 2021 by the authors. Submitted to *Universe* for possible open access publication under the terms and conditions of the Creative Commons Attribution (CC BY) license (<https://creativecommons.org/licenses/by/4.0/>).

1. A brief flashback

The first successful launch of a satellite in 1957 (Sputnik [1]) triggered a new era of astronomical observing techniques which expanded enormously the research potential in astrophysics, mainly because the terrestrial atmosphere could be overcome. Consequently, the first space observations focused on spectral regions which were not accessible from the ground. Already eight years after Sputnik, Proton satellites observed cosmic γ -rays (1965). The Orbiting Astronomical Observatory (OAO [2]) from NASA were the first operational telescopes in space. After a power failure of OAO-1 right after the launch in 1966, OAO-2 was launched in 1968, and a follow-up OAO-3 (Copernicus) in 1972. These OAO-satellites provided a wealth of insight into variability of stars and intricate details of the interstellar matter. The Astronomical Netherlands Satellite (ANS, 1974, [3]) conducted photometric observations of variable stars in the UV, followed by the NASA/ESA International Ultraviolet Explorer (IUE [4]) in 1978.

Already in the early days of space astronomy, the obvious scientific success accelerated the development of space instrumentation for all spectral ranges, taking advan-

*BRITE-CONSTELLATION was designed, built, launched, and is operated and supported by the Austrian Research Promotion Agency (FFG), the University of Vienna, the Technical University of Graz, the University of Innsbruck, the Canadian Space Agency (CSA), the University of Toronto Institute for Aerospace Studies (UTIAS), the Foundation for Polish Science & Technology (FNI TP MNiSW) and the National Science Centre (NCN).

30 tage of avoiding a turbulent and absorbing atmosphere, not to mention clouds and a
31 day/night rhythm. The desire to observe even fainter targets required launch of space
32 telescopes with increasing size - very similar to most ground based observatories. A
33 still scientifically productive example is the amazing Hubble Space Telescope (HST [5]),
34 launched in 1990.

35 It needed nearly 30 years after the dawn of space telescopes that projects explicitly
36 dedicated to “simple” stars became reality. A most prominent example is Hipparcos
37 ([6]), an ESA mission with an aperture of 29 cm, launched in 1989, with the goal to
38 determine high precision parallaxes of a large number of stars in our neighbourhood.
39 The entire sky was scanned during three years, which resulted in up to 110 data points
40 per star in the final Hipparcos and Tycho catalogues. The data have proven to be a
41 treasure chest for detecting stellar variability (Kallinger & Weiss [7] and many more).
42 The follow-up ESA mission Gaia ([8]), using a 145 x 50 cm telescope, was launched in
43 2013 and increased enormously our knowledge about the 4D picture of our Galaxy.

44 Projects in the early stages of space telescopes focused on highly ranked targets
45 devoted to evolutionary aspects of galaxies, cosmology, interstellar nebulae and their
46 role for stellar evolution, solar system planets, and other hot topics. Monitoring clas-
47 sical variable or allegedly constant stars continuously over many hours, days or even
48 months, was hindered due to the high pressure on telescope time. But fortunately, space
49 telescopes need pointing and guiding equipment, usually provided by small auxiliary
50 telescopes. One of the first star trackers, “abused” for stellar photometry, were the Fine
51 Guidance Sensors (FGS) of the HST, as is described by Kuschnig et al. [9], Kuschnig,
52 Weiss & Zwintz [10], Zwintz et al. [11], Weiss, Kuschnig & Zwintz [12], Zwintz et al.
53 [13] and in workshop proceedings of the Space Telescope Science Institute (Kuschnig,
54 Weiss & Bahr [14]).

55 But already in 1982 a first proposal for a space photometer dedicated to stellar
56 variability and activity, *Evris*, was submitted to CNES (Mangeney et al. [15]) and
57 was developed further as a passenger instrument for the USSR-Mars94 mission. It was
58 intended to be active during the cruise time to Mars (Vuillemin et al. [16]). However,
59 launch of the Mars94 mission was delayed to 1996 and ended in disaster, because
60 of a rocket failure which crashed Mars96 in the Chilean Andes together with *Evris*.
61 Fortunately, the experience gained during development of *Evris* was not lost: already
62 in 1993 the French team had submitted a larger follow-up seismology mission, *CoRoT*
63 (Schneider et al. [17], Weiss & Baglin [18]), which was launched by ESA in 2006 and
64 was active until 2014.

65 Asteroseismology experienced a boom towards the end of the last century, as it
66 became obvious how much one can learn with this tool about stellar structure and
67 evolution, as well as how one can test complex astrophysical concepts, with important
68 implications for astrophysics in general. However, excellent data were necessary for
69 such investigations, i.e. data which cover as continuously as possible a long time span
70 and with mmag accuracy or better.

71 A textbook-like example is ζ Pup (Fig. 1) which was observed simultaneously from
72 space by two satellites and which illustrates the bonus of higher photometric accuracy
73 (TESS) counter-weighted by longer data sets (BRITE). Another example is α Cir (Sec.
74 4.12 and Fig. 20). The shorter TESS run of ζ Pup has broader Fourier peaks (≈ 1.5 months
75 vs. ≈ 4.5 months long data sets), but also shows many Fourier peaks which appear to be
76 less prominent in a longer run as is illustrated in the time resolved frequency analysis
77 (lower part of Fig. 2). Evidently, stochastic stellar variability dominates in the shorter run,
78 while the 1.78 d cyclic variability of the star is much more well-defined and well-covered
79 in the longer observing run (see also Fig. 1). The changing amplitude of the 1.78 d signal
80 indicates that the signal likely is due to (bright) spots of this O4If(n) type star that come
81 and go. Sometimes the signal is not even there (see the BHr time-frequency diagram of
82 Fig. 2). Whenever there are overlapping TESS and BHr observations, they follow each
83 other relatively well and have roughly the same amplitudes, except at the beginning of

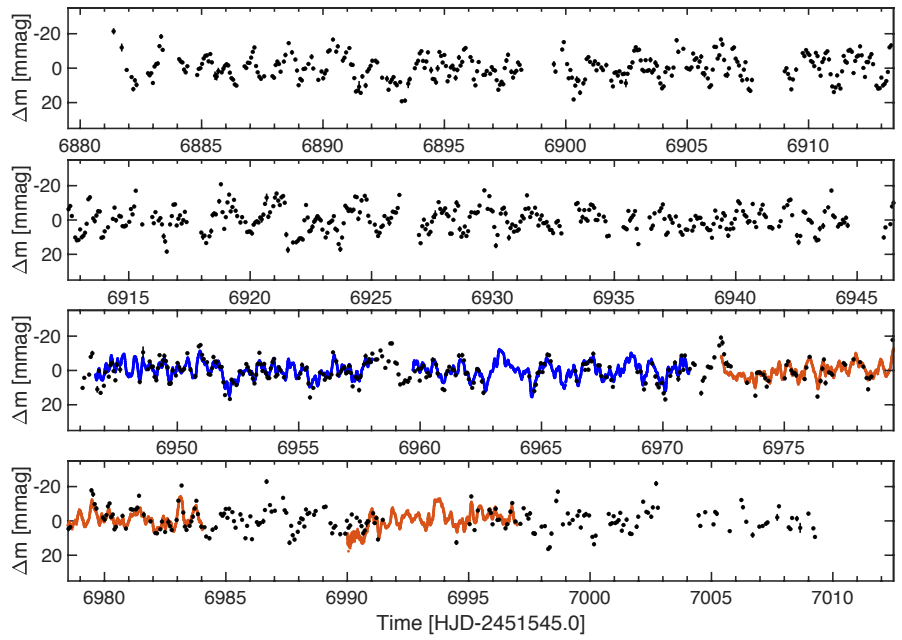


Figure 1. ζ Pup observed by BRITE-Heweliusz, a component of BRITE-CONSTELLATION, (black dots, red filter) and with TESS in sector 7 (first line in blue) and in sector 8 (second line in red).

84 each subset of the TESS observations, which is due to systematics in TESS data around
 85 gaps. More about ζ Pup is presented later in Section 4.1, including comments on the
 86 physics which probably is involved.

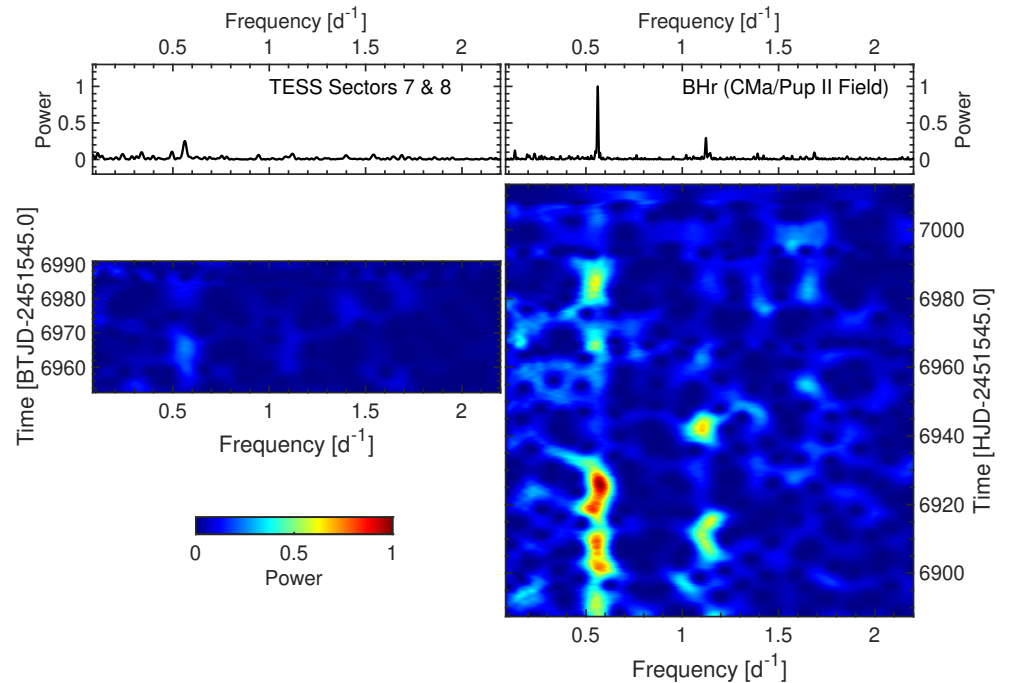


Figure 2. Time dependent frequency spectra of ζ Pup obtained from data presented in Fig. 1 (Ramiamanantsoa et al., in preparation) and with a sliding time window of 12 days. The colour scale represents signal power normalized to the maximum power in the windowed discrete Fourier transforms of the BHR data.

87 In addition to long continuous data sets, photometers operated in space have an
 88 advantage by avoiding day-time gaps in low-Earth orbits, inaccessibility of stars during

89 certain seasons, and noise introduced by a turbulent atmosphere (Weiss [19]). The need
90 for such data was subsequently boosted further by the discovery of exoplanets.

91 The CNES mission CoRoT provides a perfect example of a “small” satellite, which
92 produced top science with a rather small budget, although nowhere nearly as small as
93 that for BRITE-CONSTELLATION. Not surprisingly, the scientific community was much
94 interested in generating more such satellites, but competition with trendy space projects
95 was intense, as is illustrated by the tortuous path after CoRoT. PRISMA (Lemaire et al.
96 [20]) was developed to extend CoRoT and was accepted in 1993 as an ESA Horizon-2000
97 M2 project study, but finally lost the race in 2002 against the γ -ray satellite Integral. The
98 study team did not give up and produced a Horizon-2000 M3 proposal, STARS (Jones et
99 al. [21]), but lost again in 2009 against the cosmic background explorer Planck. The next
100 attempt was Eddington (Favata et al. [22], Roxburgh [23]), an ESA Flexi Mission, but
101 the gravitational wave detector Lisa settled its problems for a planned launch in 2015,
102 and consequently Eddington had to step back. Later, the launch of Lisa was delayed
103 and is now scheduled for 2034. But finally, Plato was proposed in 2007 and selected in
104 2014 as an ESA Cosmic Vision mission (Plato-Consortium [24]), driven by an exploding
105 interest in exoplanets. Launch is scheduled for 2026. It took 20 years after CoRoT till a
106 follow-up, Plato, finally was decided and about 30 years till - hopefully - first data will
107 be available!

108 Outside Europe similar efforts were also successful. Soon after the crash of Evris,
109 an Announcement of Opportunity (AO) for Small Payloads was distributed in 1996 by
110 the Canadian Space Agency (CSA), which was responded to in 1997 with a proposal for
111 MOST (Rucinski et al. [25]). This satellite was launched in 2003 as Canada’s first space
112 telescope, and with an aperture of 15 cm it was the smallest space telescope in orbit at
113 that time. While designed only for a nominal lifetime of one year, it collected under the
114 directorship of Jaymie Matthews (UBC) scientifically useful data till January 2018, i.e.
115 for more than 15 years! Even after the CSA operations, funding ended in 2014, MOST
116 was frequently activated for pay-per-view observers.

117 Paying tribute to the exploding interest in exoplanets after the detection of 51b Peg,
118 NASA decided in 2001 to fund a space telescope, Kepler, dedicated to the discovery
119 of exoplanets (Borucki et al. [26]). At that time only 80 exoplanets were known, a
120 number which increased dramatically after Kepler’s launch in 2009. Reaction-wheel
121 failures in 2012 and 2013 resulted in a modified mission, Kepler-K2, which finally ended
122 the mission in 2018, after discovery of more than 2,600 exoplanets and delivering an
123 enormous amount of data for asteroseismology.

124 The Wide Field Infrared Explorer (WIRE) reminds one of the HST’s Fine Guidance
125 Sensors as auxiliary equipment with a potential for space photometry. WIRE (Hacking
126 et al. [32]) was launched in 1999, but due to a premature ejection of the telescope
127 cover, all cryogen quickly evaporated and made IR observation impossible. Fortunately,
128 the star tracker was still working and contributed successfully to asteroseismology till
129 decommissioning of WIRE in 2011. This exceeded substantially the 4 months of the
130 originally planned life time of the IR mission. Another mission producing photometric
131 data for asteroseismology as a side-product to its main research goal is the Solar Mass
132 Ejection Imager (SMEI) on board of Coriolis (Eyles et al. [33]), which was operational
133 from 2003 to 2011 in a sun synchronous polar orbit with 102 min period.

134 The follow-up mission to Kepler is TESS, which was first discussed in 2005 and
135 launched in 2018 by NASA, just after ending the Kepler mission. TESS (Ricker et al.
136 [27]) focusses on the stars brighter than those observed by Kepler and the K2 follow-up,
137 and it covers a sky area 400 times larger than that monitored by Kepler. As an example
138 of the relevance of TESS data for asteroseismology we refer, e.g., to Cunha et al. [28],
139 Antoci et al. [29], Bowman D.M. [30] and Burssens et al. [31].

140 More information about HST, Kepler, Gaia and TESS will be presented in dedi-
141 cated chapters of this journal volume.

142 2. The birth of BRITE-Constellation

143 The development of BRITE-CONSTELLATION can be traced to the origins of the
144 Canadian microsatellite MOST [25], which was designed by Slavek Rucinski and Kieran
145 Carroll (University of Toronto, UT), starting with construction in 1998, and successfully
146 utilized by the team led by Jaymie Matthews (UBC) after launch in 2003 till 2014. Robert
147 Zee (Manager of UT Space Flight Laboratory, SFL) wanted to continue the momentum
148 created by the success of MOST and asked Rucinski in 2002 the non-trivial question,
149 if nanosatellites could be of relevance for astronomy. One has to keep in mind that
150 at that time nanosatellites were young and rarely utilized for research, with primary
151 interest as an engineering experimentation exercise and looking down, not up, for Earth-
152 atmosphere and -surface research. Nevertheless, a design concept for a single CANX-3
153 satellite was developed in 2004 by SFL and a small team of Canadian astronomers as a
154 first fully three-axis stabilized satellite of $20 \times 20 \times 20$ cm size, containing a telescope with
155 3 cm aperture (Fig. 3).

156 Another root of origin is with Werner Weiss (University of Vienna, UoV) who
157 was co-I of Evris, later of CoRoT and also member of the MOST team. The latter
158 membership closed the loop to CANX-3. The failure of the Evris-launch contrasted
159 dramatically with the anticipated research potential for asteroseismology, an expectation
160 which later was confirmed by CoRoT and MOST. Hence, the pressure to produce a
161 space telescope optimised for bright stars grew. Luckily, the Austrian Ministry of Science
162 and Technology established in March 2005 a program for improving the infrastructure
163 of Austrian Universities, to which UoV submitted a proposal for UNIBRITE. This was
164 accepted in October 2005, and one month later, UNIBRITE was ordered at SFL, based on
165 their concept of CANX-3.

166 A third root is with Otto Koudelka (Technical University Graz, TUG). The Austrian
167 Space Agency (ASA) issued in 2005 a call for the 3rd Austrian Space Programme. Two
168 nanosatellite proposals were in the queue: one of the Institute for Astrophysics (UoV),
169 dedicated to asteroseismology (Weiss [19]), and another from the Institute of Communi-
170 cation Networks and Satellite Communications (TUG), for developing and building a
171 cubesat. ASA suggested to merge these initiatives, which resulted in a proposal with
172 Koudelka at TUG as the PI, and which was approved by ASA in 2006. This was the birth
173 of the first satellite built in Graz (and Austria): BRITE-AUSTRIA, also called TUGSAT-1.
174 The link to MOST is highlighted in a sentence of the proposal: BRITE-AUSTRIA will
175 extend and supplement the spectacularly successful Canadian microsatellite MOST into
176 the domain of nanosatellites.

177 As the Austrian BRITE's were accepted for funding, Slavek Rucinski felt that
178 Poland (his country of birth) with its rapidly improving economy should join. When
179 the Canadian part of the project appeared to be in limbo due to CSA dragging its heels
180 regarding funding (from 2006 until 2011), he started pushing his colleagues and former
181 students in Poland to follow the Austrian example. Aleksander Schwarzenberg-Czerny
182 (Copernicus Astronomical Center, Warsaw, CAMK and former PhD student of Rucinski)
183 was able to obtain funding for two BRITE satellites at the end of 2009 and, hence, he
184 provides the fourth root of BRITE-CONSTELLATION.

185 The pressure on the Canadian Space Agency (CSA) increased considerably, after
186 Austria funded UNIBRITE and BRITE-AUSTRIA, and after Poland funded BRITE-
187 HEWELIUSZ and BRITE-LEM. Finally, CSA accepted in 2011 the two Canadian BRITE's
188 (former CANX-3): BRITE-TORONTO and BRITE-MONTREAL.

189 And in this way BRITE-CONSTELLATION was born with six satellites.

190 3. BRITE-Constellation

191 The goal of BRITE-CONSTELLATION [34] was to provide high-precision photomet-
192 ric monitoring of very bright ($\lesssim 4$ mag) stars in two optical wavelength bands (colours),
193 i.e. blue and red, and for up to 6 months, the maximum feasible time in an affordable
194 low-Earth orbit. Various concepts have been discussed and finally a single telescope,

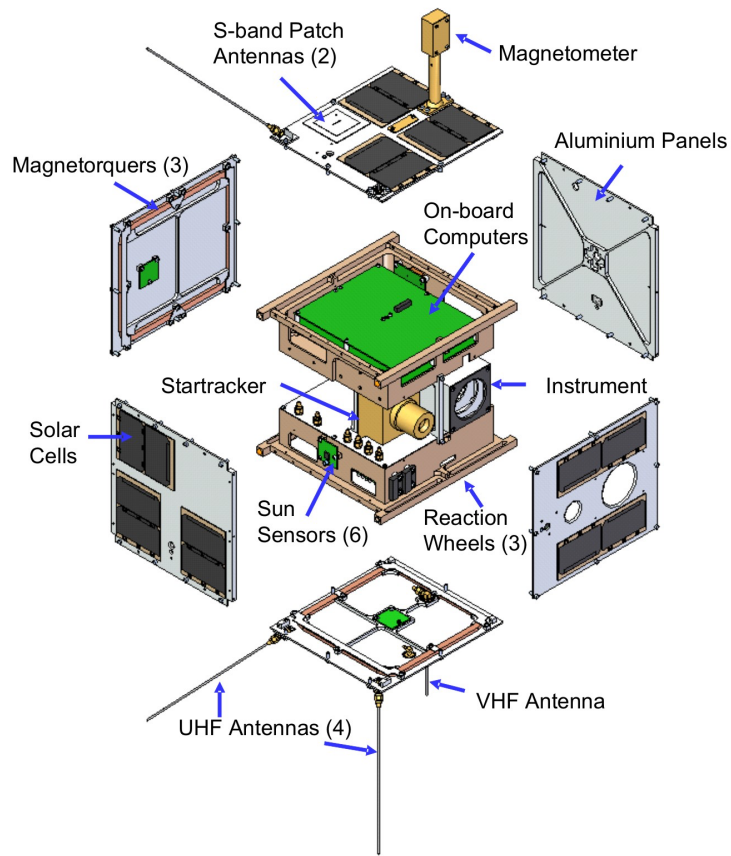


Figure 3. Basic structure of the BRITE satellites. Source: SFL

195 optimized for a given passband was chosen with no moving elements on board, thus
 196 reducing risk, but which required one spacecraft per filter.

197 The proceedings of the First BRITE Workshop ([35]) provide an overview to the
 198 technical and scientific issues which were discussed and decided before launch in 2013.
 199 The situation of the six (five active) components of BRITE-CONSTELLATION after launch
 200 (Table 1) are described in Weiss et al. [36], Deschamps et al. [37], Koudelka et al. [38] and
 201 various aspects of BRITE-data reduction in Pablo [39], Popowicz et al. [40], Popowicz
 202 [41].

203 Nearly each year conferences were organised to discuss updates and new aspects of
 204 the mission. Most important, they allowed for vivid scientific discussions which helped
 205 to shape the focus of BRITE-CONSTELLATION. The first science conference took place in
 206 2015 in Gdańsk, Poland, one year later in Innsbruck ([42]), and in 2017 at Lac Taureau,
 207 Canada. The conference in Vienna “Stars and their Variability, Observed from Space -
 208 Celebrating the 5th Anniversary of BRITE-CONSTELLATION” in August 2019 provides
 209 the most recent status report [43].

210 3.1. Instrumentation

211 The BRITE instruments consist of a multi-lens telescope with an aperture of 3 cm,
 212 optimised for the red (550 – 700 nm) or the blue (400 – 450 nm) wavelength range (Fig.
 213 4, red design). The unvignetted field of view (FOV) is about 24° in diameter and the
 214 optics were chosen to provide slightly out-of-focus stellar images for improved S/N,
 215 an experience acquired from MOST. For the two Austrian, the two Canadian and the
 216 blue Polish instruments a 5-lens system was developed. The red Polish instrument (BHR)
 217 has a four-lens design, which results in a shorter telescope, but with a smaller FOV of
 218 20°. A baffle in front of each telescope reduces off-axis stray-light from bright sources,
 219 including the Sun, Moon and Earth.

Owner	Name	Filter	ID	Launch Date	Orbit km	Period min
Austria	UNI-BRITE	red	UBr	25 Feb. 2013	781 × 766	100.37
	BRITE-AUSTRIA	blue	BAb	25 Feb. 2013	781 × 766	100.36
Poland	BRITE-HEWELIUSZ	red	BHr	19 Aug. 2014	612 × 640	97.10
	BRITE-LEM	blue	BLb	21 Nov. 2013	600 × 900	99.57
Canada	BRITE-TORONTO	red	BTr	19 June 2014	629 × 577	98.24
	<i>BRITE-Montréal</i>	<i>blue</i>		<i>19 June 2014</i>		<i>n/a</i>

Table 1: Launch and orbital information for the BRITE nanosats. BRITE-MONTRÉAL did not separate from the launch vehicle and is not operational. The red filter covers 550 – 700 nm, and the blue filter 400 – 450 nm.

220 The same interline frame-transfer CCDs, a Kodak KAI 11002-M (4048 × 2672 pixels
 221 and 9 μm pixel size) chip, are used for each BRITE. This is an off-the-shelf product which
 222 includes all read-out electronics and preamplifiers on a header board behind the chip.
 223 Attractive features, besides the modest price, is the low dark current at high temperatures
 224 (0° – 30° C), which allows one to avoid a cooling system, and a low read-noise and power
 225 consumption. This CCD has been successfully used on the ground in SBIG Cameras,
 226 but never in the radiation environment of space. In order to avoid pixel saturation, the
 227 CCD is positioned out-of-focus, which together with the optical design results in about
 228 8-pixel-wide on-axis stellar images. Off-center images have a more complex shape, as is
 229 shown in Fig. 5. The scale is about 27" – 30" per pixel, increasing slightly towards the
 230 edge due to image distortion.

231 3.2. Photometry and data processing

232 The BRITE mission requirements were set in 2005 such that the instruments shall
 233 observe a selected star-field for at least 15 minutes per orbit. Outside that time interval,
 234 scattered light from the Earth and Sun would be encountered. Data from up to 15 stars
 235 per field shall be collected for up to 100 days. In reality the BRITE satellites typically
 236 collect data from 24 to 28 stars during 20 to 40 minutes per orbit over a time base of
 237 about 160 days. The exposure times typically vary between 1 and 5 seconds and every
 238 21 seconds subframes were read out. All functioning BRITE satellites were launched
 239 into low-earth polar orbits with periods close to 100 minutes.

240 Target fields can be occulted by the Earth during part of the orbit. After the field
 241 becomes visible again and its distance from the earth-limb exceeds a critical angle, the
 242 Attitude Control System (ACS) of the satellite re-points the star field in the camera
 243 FOV. To obtain top-quality photometry, the ACS must assure stable pointing of the PSF
 244 during the entire observing run close to the same pixels (flat-field exposures are not

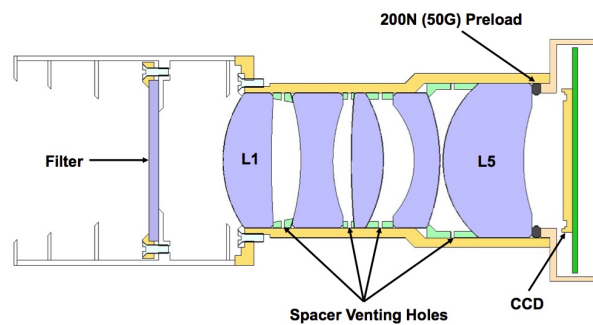


Figure 4. Camera scheme for the UNIBRITE and BRITE-TORONTO red instruments with a nearly vignetting free field-of-view of 24°. The red or blue filters are placed at the entrance pupil of the 5-lens camera to assure a constant filter function over the entire FOV. The blue cameras have slightly modified lens radii and separations to optimise the image quality for the needed wavelength range. Source: SFL

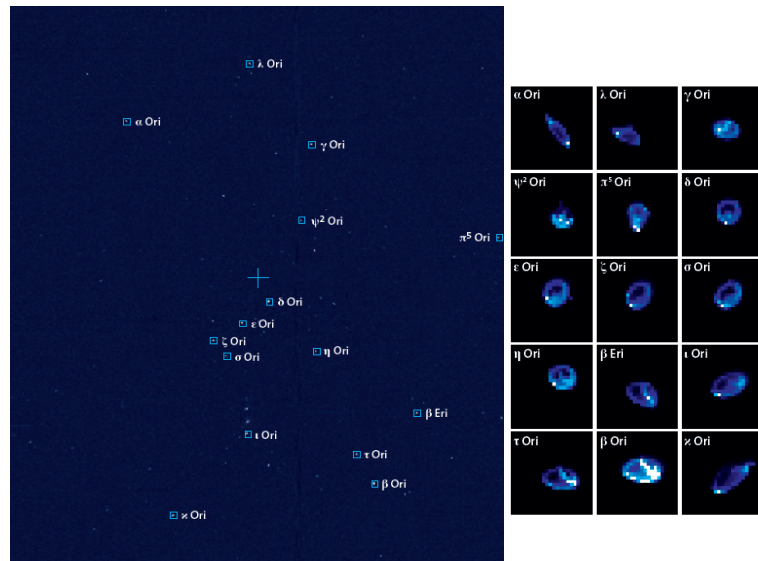


Figure 5. Full frame image of the Orion field taken with UniBRITE (UBr) in December 2013. The stars which have been selected for photometric time series are indicated. Subframes (24 x 24 pixels) which contain a full PSF, were stored in memory for a later download to the ground. Typical subframes in the center and close to the edge of the field are presented in the right panel.

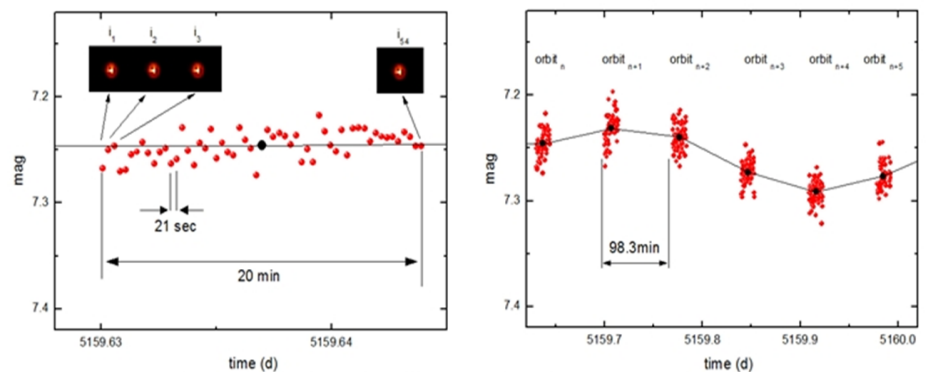


Figure 6. A typical photometric sequence of 44 Cyg (Zwintz [44]), observed by BRITE-Toronto in the field during a single orbit (left) and the data sequence during six consecutive orbits (right), indicating intrinsic light variations.

245 possible), which typically is achieved within 1.5' rms (≈ 3 pixels). An example of such a
 246 photometric cadence is show in Fig. 6. Whenever possible, a satellite setup was chosen
 247 allowing one to observe a second field during an orbit, when the first field was invisible
 248 for the satellite.

249 After the first BRITE satellites (UBr and BAb) were launched and first images
 250 were recorded, features appeared which were not present in the laboratory: pixels
 251 and even entire columns with increased dark (thermal) signal, i.e. “hot pixels” and
 252 “warm columns” (Fig. 7). These flaws were distributed over a significant fraction of the
 253 CCD, in the FOV as well as outside with no light access. The defects became stronger
 254 during successive weeks, even at the same CCD operating temperature. The signal of
 255 “warm columns” ranged from 100 to 500 ADUs above nominal background. One ADU
 256 corresponds at 20° C to 3.2 detected electrons. For a “hot” pixel the signal (even without
 257 illumination) is more than 100 ADUs above median background and it can get even close
 258 to saturation (≈ 1200 ADUs). All BRITE satellites suffer these radiation defects, believed
 259 to arise mainly from proton collisions, which accumulate over time and adversely affect
 260 the data reduction and quality.

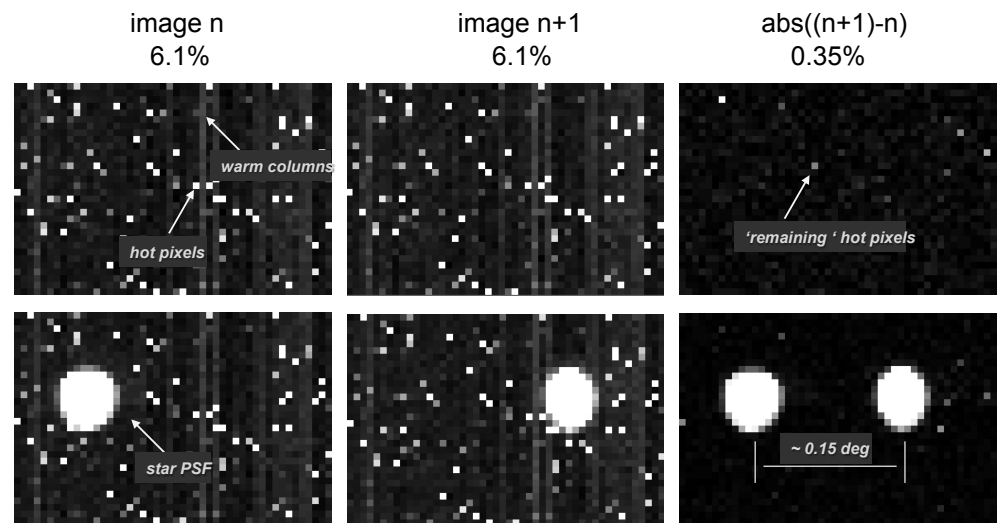


Figure 7. Illustration of the chopping procedure. Top: empty rasters (24×36 pixel subsets of a frame). The left and middle raster was off-set horizontally by about 0.15° . Bottom: same as for top row, but with the telescope moved to a nearby star in the raster. Right column: absolute values of the raster differences. All images here were taken at about $+20^\circ\text{C}$ operating temperature. The values on top of the upper row are the % of pixels which reveal a dark current higher than 100 ADU, compared to the median background of all pixels in the respective raster.

261 As is described in [40,41], a very efficient technique to overcome the mentioned
 262 detector flaws and to improve significantly the accuracy of the CCD photometry is the
 263 “chopping” technique, which was introduced to the observing procedure in November
 264 2014 and installed in February 2015 as default observing mode for all satellites. This
 265 mode replaced the previously used “stare” mode. In the chopping mode a satellite is
 266 shifted between exposures back and forth, so that for every second raster-image the
 267 star is positioned in the other part of the raster (Fig. 7). Finally, the difference of two
 268 subsequent rasters contains essentially only information relating to the stellar brightness
 269 and all local background features are close to being eliminated.

270 Data reduction of all BRITE photometry is the responsibility of the Data Reduction
 271 and Quality Control (DRQC) team (see Subsection 3.3). The data corrected for, e.g., the
 272 flux values with the CCD temperature and x and y pointing positions on the CCD, are
 273 archived and forwarded to the Principal Investigators (PI) for further decorrelation. De-
 274 correlation methods have been developed by Pigulski and documented as the “BRITE
 275 Cookbook”, which can be accessed together with the software code at
 276 <https://www.pta.edu.pl/pliki/proc/vol8/v8p175.pdf>.
 277 Examples of BRITE photometry are presented in Figs. 6, 13, 14, 15, 16, 18, 21 and 23.

278 3.3. Organisation and operation

279 Organisation and operation of BRITE-CONSTELLATION relies on six interacting
 280 teams (Fig. 8), which are:

- 281 • BEST (BRITE Executive Science Team) is the ruling body of BRITE-CONSTELLATION.
 282 It consists of 2 voting members per satellite, nominated by the three member countries
 283 (Austria, Canada and Poland) which funded the BRITE satellites. BEST elects additional
 284 non-voting experts, presently 15. BEST releases 6 to 12 months before a new observing
 285 campaigns starts a BRITE Observing Plan (BOP), which typically covers 12 to 14 months
 286 of operation. The BOP defines which satellite is assigned to which field and for how long
 287 (Figs. 9 and 10). The rather long lead-time allows the PI’s to organise supplementary
 288 observations from the ground or from space.
- 289 • MC (Mission Control) team is headed by Rainer Kuschnig (IKS, TU-Graz, formerly IfA
 290 Uni-Vienna) and is responsible for the execution of BOP by providing satellite orientation

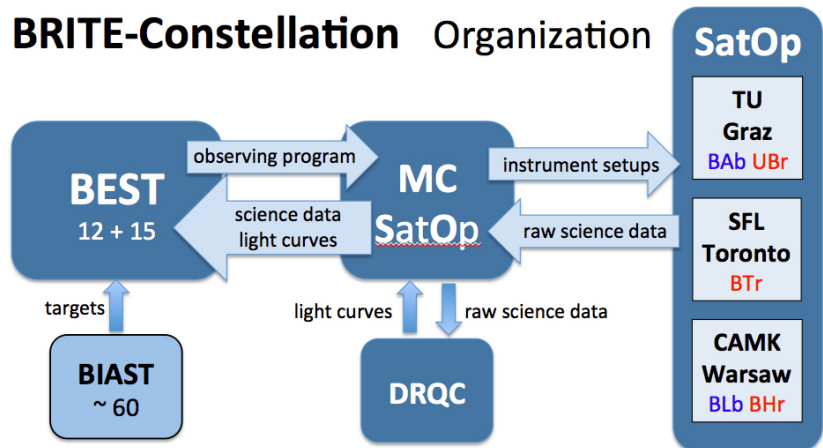


Figure 8. Organisation structure of BRITE-CONSTELLATION. BEST: BRITE Executive Science Team, MC: Mission Control, SatOp: Satellite Operation, DRQC: Data Reduction & Quality Control, BIAST: BRITE International Advisory Science Team

291 and instrument setup data. To ensure a maximum efficiency of BRITE-CONSTELLATION,
 292 a frequent quality control of all data generated with all active satellites is another core
 293 activity of MC. Such tests are applied at least twice a week and reported to BEST every
 294 second week. In case of problems, MC interacts directly with the corresponding satellite
 295 operator in charge.

296 A very short turn-around time between data check and satellite operation is possible,
 297 because BRITE-CONSTELLATION observes “only” up to 60 stars during a campaign and
 298 basically a single person inspects the data nearly in real time. The obvious benefit is a fast
 299 response to unexpected stellar variability. The best and most outstanding example is the
 300 serendipitous data collection from NOVA Carinae 2018. Almost instantly it was apparent
 301 that BRITE-CONSTELLATION had caught the nova days before it was discovered visually.
 302 Hence, this early volatile phase could be covered by BRITE-CONSTELLATION in an
 303 unprecedented manner, as is explained in Section 4.16.

304 • SatOp (Satellite Operation) teams are other key elements of the mission. Satellite
 305 operators are in charge of controlling the national spacecraft via the ground stations, of
 306 which one is in Austria at TU-Graz, one in Canada at SFL-Toronto and a third one in
 307 Poland at CAMK-Warsaw. However, in case of emergency, communication is possible
 308 from each of the ground stations to any satellite to ensure uninterrupted satellite control
 309 and data management. This was and still is usually required during harsh weather
 310 conditions at particular ground stations or during maintenance periods.

311 • DRQC (Data Reduction and Quality Control) is another core element of the mission.
 312 The data received from each BRITE satellite on a daily basis is delivered by SatOp to
 313 MC for a preliminary quality check. Once a campaign on a given field is finished, all
 314 raw data are ASCII formatted with a FITS-like header and made available to DRQC,
 315 which generates pipeline-reduced data files (supervised by Adam Popowicz, Silesian
 316 University of Technology, Gliwice) [40], and performs quality control (supervised by
 317 Bert Pablo, AAVSO). The original data, the raw science data (ASCII) files and the time
 318 series datasets are then submitted to the BRITE Data Archive (maintained by Andrzej
 319 Pigulski, University of Wroclaw). Most of the archive can be accessed publicly, but some
 320 data are still protected for a limited time for the corresponding PIs. The BRITE Public
 321 Data Archive can be found at <https://brite.camk.edu.pl/pub/index.html>.

322 • BIAST (BRITE International Advisory Science Team) is an informal group of presently
 323 60 scientists, who have already successfully proposed relevant observations and/or are
 324 planning this in the future. Hence, BIAST members have expertise in BRITE data, have
 325 published the results and can advise BEST in optimising the observing program.

326 • GBOT (Ground-Based Observing Team), which is headed by Konstanze Zwintz

327 (U. Innsbruck), provides a platform for BRITE scientists and observers worldwide to
 328 support collaboration and to maximize the scientific output of BRITE-CONSTELLATION.

329 3.4. Present Status

330 The various star fields observed with various BRITE satellites since launch and
 331 until 2020 are presented in Fig. 9. Which satellite observed a field in which period, either
 332 in chopping or stare mode, is indicated in Fig. 10.

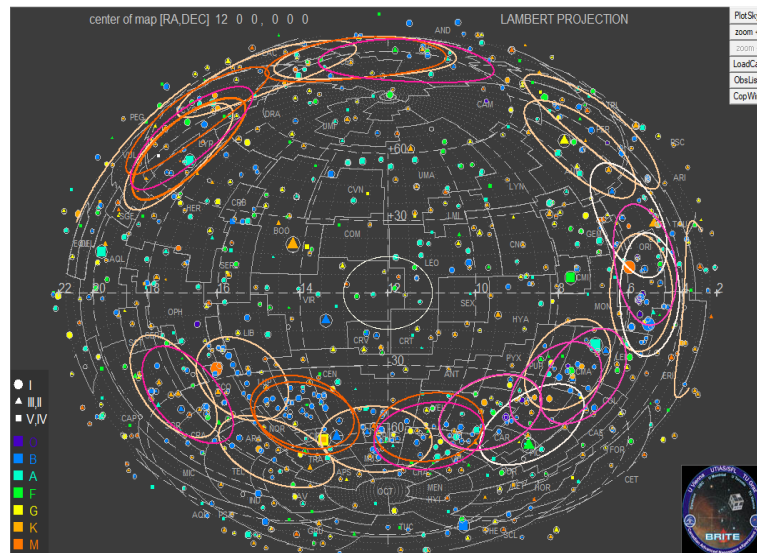


Figure 9. Sky map highlighting the fields observed thus far by at least one BRITE satellite.

333 As of March 2021, 705 individual stars have been observed so far, often contemporane-
 334 ously in two colours, and almost 6 million image-rasters of target stars have been
 335 produced. Most observations occurred in fields close to the Galactic plane, where the
 336 density of very bright stars in the FOV is high, allowing a proper choice of guide stars
 337 by the much less sensitive guiding telescope (Fig. 9). Also many of the primary targets
 338 listed in the early BRITE proposals were located in this area, e.g., the bright OB, B and
 339 Be stars in Orion, Carina, Centaurus or Sagittarius.

340 The observing strategy of BEST during the past 8 years focused not only on stars
 341 of primary interest to the BRITE-community, like 6-month campaigns on hot, massive
 342 and intrinsically bright stars, but also to re-observe high profile targets essentially every
 343 possible season. The best examples are the brightest stars in the Orion field, which have
 344 been selected for the first campaign starting in December 2013 and which are currently
 345 being observed for the 8th time (Fig. 10). These datasets are certainly jewels of the
 346 BRITE-CONSTELLATION legacy program.

347 Even though the early BRITE science program focused on O to B (including Be)
 348 type stars, it also includes now objects beyond this range in the HR diagram (Fig. 12),
 349 which is indebted to wide field photometry, reaching by default many stars and of
 350 different type. For example, cool red-giants have been observed, although not originally
 351 considered a priority, but the first data analysis led already to a relevant publication. An
 352 excellent example is β Pictoris (Section 4.11). Finally it should be mentioned that TESS
 353 obtained data for stars which BRITE satellites observed simultaneously. An example
 354 was already given in Section 1 with ζ Puppis.

355 For all BRITE satellites the nominal lifetime was two years. Hence, the still active
 356 satellites exceed this limit more than three times, which illustrates the high engineer-
 357 ing quality. Nevertheless, BRITE-CONSTELLATION encountered technical problems
 358 described in the following.

359 The photometric accuracy is limited primarily due to stabilisation problems of
 360 BRITE satellites, but also by problems related to increasing CCD defects (Popowicz

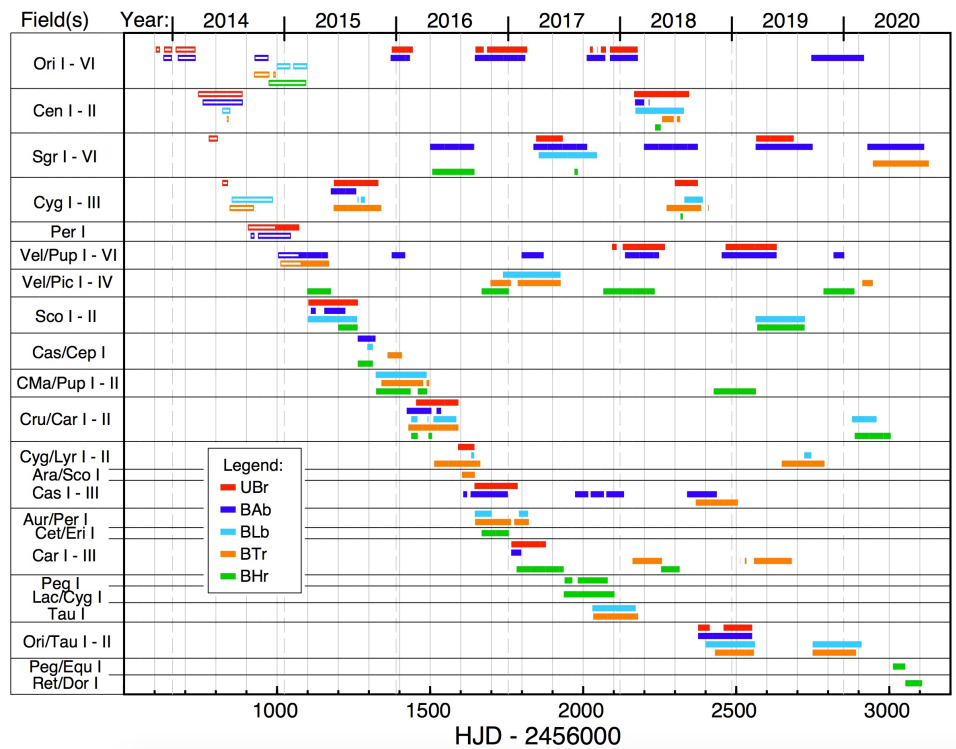


Figure 10. Temporal distribution of the observations of all five active BRITE satellites until the end of 2020. The data obtained in the stare and chopping observing modes are shown with unfilled and filled bars, respectively.

361 [45], Popowicz & Farah [46]). The development, e.g., of the normalised detector dark
 362 current with time is presented in Fig. 11. Obviously, satellites with either a tungsten or a
 363 light weight borotron shield suffer significantly lower thermal noise increase compared
 364 to unshielded CCDs. Moreover, the sensors probably received different radiation doses
 during launch, as is indicated in Fig. 11 by the onset of the linear approximations.

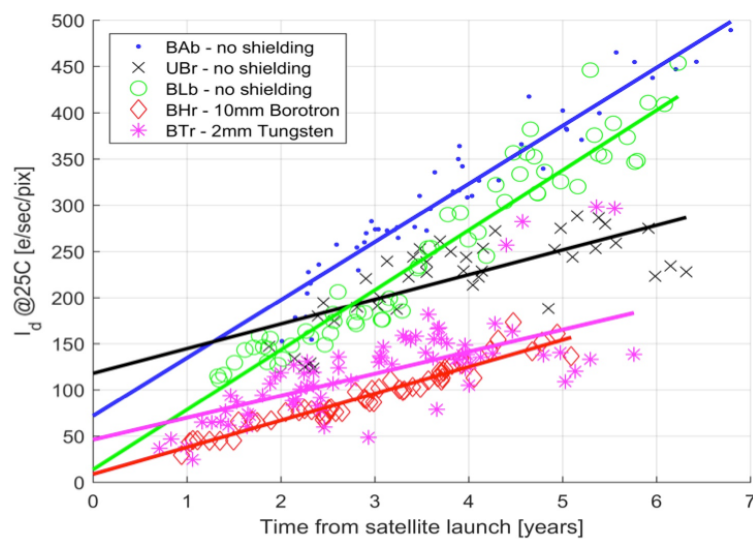


Figure 11. Temporal development of the CCD dark currents.

365

366 The status of individual BRITE satellites can be summarized as:

- 367 • BRITE-Toronto (BTr), is in good condition and produces among the best data, despite
- 368 a significant amount of radiation damage. Primary target stars can be placed on the CCD

369 where the background is least noisy.

370 • BRITE-Heweliusz (BHr), is working very well in general; some observing fields seem
371 to cause problems for the pointing system, but usually alternative orientations of the
372 field (different guide stars) can be chosen. It also has the least amount of radiation
373 damage due to a better shielding of the CCD.

374 • BRITE-AUSTRIA (BAb) produces scientifically relevant data, even after more than
375 eight years in orbit and an enhanced radiation environment. To obtain the best photo-
376 metric consistency over the lifetime of BRITE-CONSTELLATION, this satellite has been
377 assigned to observe every year essentially the same set of fields in Orion and Sagittarius.

378 • UniBRITE (UBr), was working well until June 2019, despite its high grade of radia-
379 tion damage. However, it failed after that date and a failure analysis led by SFL and
380 conducted by IKS TU-Graz concluded that one of the three reaction wheels seems to be
381 damaged and cannot be used for stabilising the spacecraft. A repair concept is being
382 developed.

383 • BRITE-Lem (BLb), worked well until April 2020 when it consistently failed to get into
384 fine pointing. This is very likely due to a damaged reaction wheel. However more tests
385 are still to be conducted to come to a firm decision.

386 In conclusion, presently three of the five functioning BRITE-CONSTELLATION
387 satellites are still operational: BHr and BTr are producing very good data and BAb still
388 useful photometry. BEST expects to continue the mission until at least in 2022, depending
389 on unpredictable technical failures, e.g., of the reaction wheels. Attempts to recover the
390 other two BRITES will continue.

391 4. Key results of the mission and scientific highlights

392 Since its launch BRITE-CONSTELLATION has obtained measurements for 705 in-
393 dividual targets in 60 currently completed fields (Fig. 9) of which many overlap. A
394 large fraction of the targets was observed in more than one field which yields total time
395 bases of up to eight years for several stars (Fig. 10). As of March 2021, 11.5% of all
396 targets observed by BRITE-CONSTELLATION are included in one or more peer-reviewed
397 publications. BRITE data of many other targets are still being actively analyzed and will
398 be the topics of additional future papers. In the following, selected research highlights
399 based on BRITE-CONSTELLATION data are presented, mostly sorted from most massive
400 to least massive stars. The individual objects are also indicated in Fig. 12.

401 4.1. The link between stellar and wind variability in very massive stars

402 High-precision photometry of the runaway early-O-type supergiant ζ Puppis (Figs.
403 1, 2 and 13) revealed that a previously-proposed rotation period of 5.1 d is incorrect
404 and the period actually is 1.78 d, which agrees much better with a model for the rota-
405 tional evolution. Figure 13 also indicates that the large, real scatter beyond the 1.78 d
406 modulation, is probably due to stochastically varying short-lived bright regions in the
407 photosphere arising in a subsurface convection zone, which lead to clumps in the wind.
408 An alternative supposition is that the stochastic variability arises from gravity waves at
409 the internal radiative/convection border. This is supported by hydrodynamic simula-
410 tions showing gravity waves causing stochastic variability in the photospheres of main
411 sequence OB stars (Bowman et al. [48]).

412 The top diagram in the right column of Fig. 13 shows that both kinds of bright
413 spots show the same variability amplitude in the BRITE blue and red filters, implying
414 insensitivity to the expected hotter nature of the spots compared to their adjacent areas
415 in the stellar photosphere. The reason for this is that the Rayleigh-Jeans tails of the stellar
416 emission spectrum are sampled at significantly longer wavelengths, compared to the
417 UV maximum peak. The bottom diagram in the right column is consistent with the
418 photometric precision of the data.

419 The findings yielded by the 2014/2015 observing campaign on ζ Puppis may be an
420 important resolution of a long-standing puzzle indicating subsurface convection as the

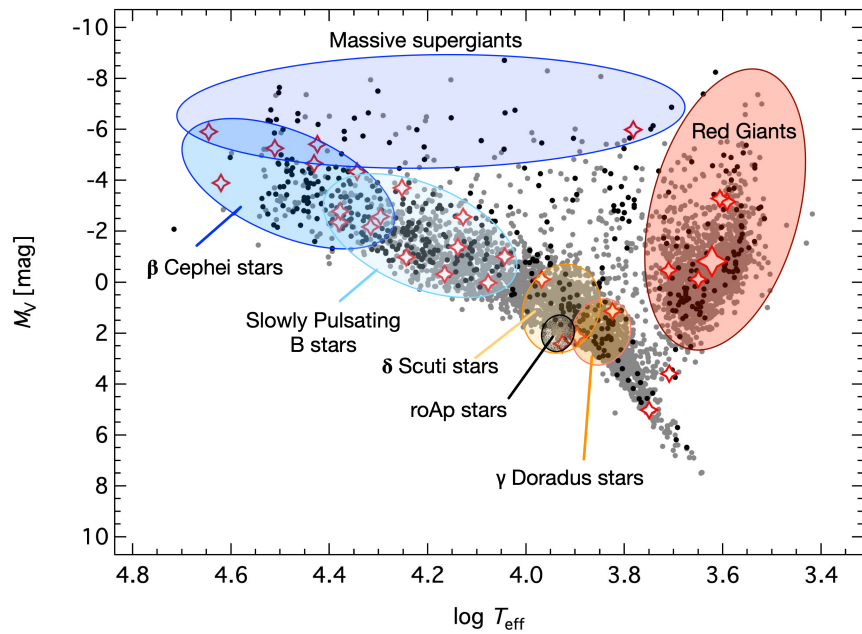


Figure 12. HR diagram of the stars brighter than 6 mag in V (grey dots). Stars for which BRITE photometry was collected are shown by black dots. The objects discussed in Section 4 are marked as open red symbols where the larger symbol stands as a representation of the 23 red giants discussed in Section 4.15. Indicative instability domains for several types of pulsators are shown as colored ellipses. Be stars cover much of the β Cep and SPB domains

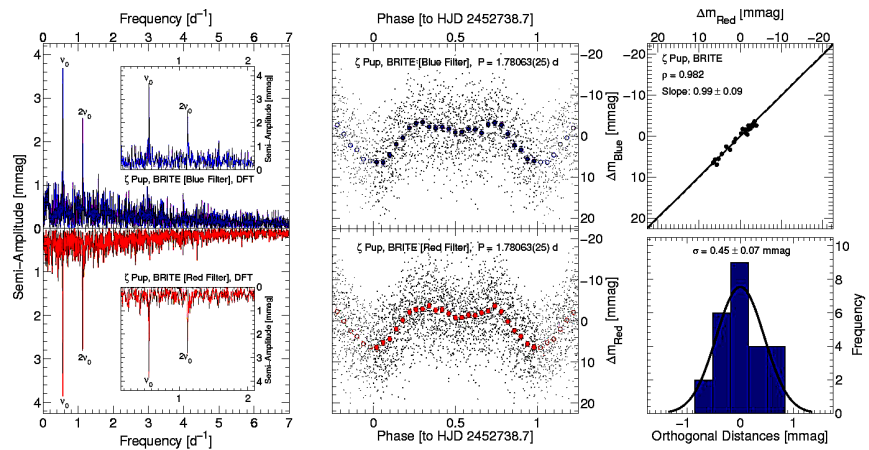


Figure 13. Left: Fourier transform of the red and blue 2014/15 BRITE photometry of ζ Puppis (see Fig. 10 for VelPup I-VI runs). Middle: Corresponding rotation light curve ($P=1.78$ d). Coloured points are 0.04 phase bins with 1σ error. Note the large, real scatter, which could be due to stochastically varying short-lived bright regions in the photosphere which lead to clumps in the wind. Right: Comparison diagram for the phased blue and red light curves (top), and distribution of orthogonal distances with a Gaussian fit (bottom). (Fig. 5 of Ramiamanantsoa et al. [47])

421 main source of the two types of wind variability (quasi-periodic co-rotating interaction
422 regions - CIRs - and stochastic clumps), which previously was not considered possible
423 in such hot stars.

424 After this study of ζ Puppis, parallel observations were obtained in 2018/19 using
425 BRITE in the optical and Chandra in X-rays (Nichols et al. [49]). Both satellites confirm
426 a 1.78 d period (Fig. 14), which is thought to be the result of bright photospheric spots

427 driving CIRs in the stellar wind, with the X-rays arising somewhat further out in the
 428 wind, where the CIR shock is strongest. Alternatively, as noted above, the stochastic
 429 component of variability could arise from gravity waves arriving from a much deeper
 430 zone.

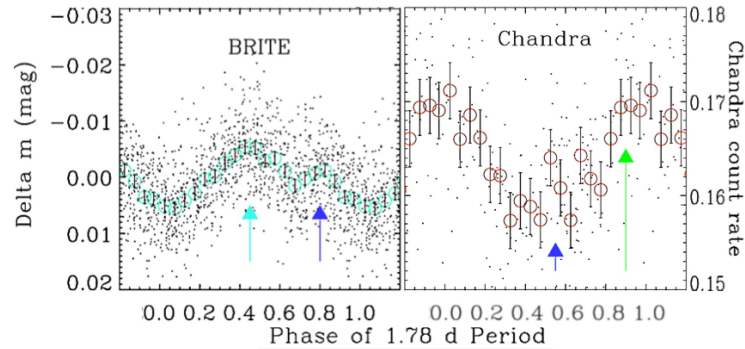


Figure 14. ζ Puppis observed in the visible with BRITE and in X-rays with Chandra, folded with the period of 1.78 d. The multi-wavelength light curve behaviour presumably illustrates the effects of Corotating Interaction Regions. The cyan arrows indicate the primary and the blue arrows the secondary maximum. There is a significant shift in the times of maximum due to a large delay or a smaller shift but mismatch in which is primary and secondary maximum (Fig. 3 of Nichols et al. [49]).

431 A very recent investigation was made on about 60 bright galactic Wolf-Rayet
 432 stars using combined data sets from MOST, BRITE and TESS by Lenoir-Craig et al.
 433 (submitted to ApJ and in [50]). Fourier analysis of the light curves reveals an important
 434 trend of enhanced stochastic variability at low frequencies ($\lesssim 1 \text{ cd}^{-1}$) with the spectrally-
 435 modelled hydrostatic-core temperatures (T^*), much like a preceding ground-based
 436 spectral variability study by Chené et al. [51,52]. Both studies support the idea that the
 437 stochastic variability seen in all WR stars arises in clump formation and propagation
 438 in their strong winds, such that, surprisingly, hotter WR stars with faster winds show
 439 less variability and hence less clumping. This can be explained by the triggering of the
 440 clumps in subsurface convective zones that are deeper and stronger in cooler WR stars.
 441 This may or may not conflict with the heretofore theory of clump formation by wind
 442 instabilities, which are expected to be stronger in hotter, faster WR winds.

443 Other targets with similar science relevance are WR 40 (WN8h; Ramiaramanantsoa
 444 et al. [53]), V973 Sco (O8Iaf; Ramiaramanantsoa et al. [54]) and γ^2 Vel (WC8+O7.5III-V;
 445 Richardson et al. [55]). They were among those prominently observed by BRITE-
 446 CONSTELLATION during several runs and helped to investigate the dynamics of winds
 447 and their relation to variations occurring at the stellar (hydrostatic) surface.

448 4.2. The heartbeat of stars: ι Orionis and ϵ Lupi

449 Heartbeat stars are a class of eccentric binaries which are characterized by tidally
 450 excited oscillations (TEO) with distinct amplitude changes at periastron. They are
 451 uniquely interesting for the study of massive stars, because they allow for full binary
 452 solutions without eclipses and provide access to asteroseismology of objects where
 453 pulsation is rare. Using BRITE-CONSTELLATION, the well-studied binary system ι Ori
 454 (O9III+B1 III/IV) was the first massive star ever in which TEOs were discovered, and
 455 which opened a whole new avenue to studying massive star interiors (Pablo et al. [56]).
 456 The data in Fig.15 are phased to periastron (phase = 1.0, with $P = 29.13376 \text{ d}$) and binned
 457 to 0.0025 in phase.

458 Another unique heartbeat star discovered with BRITE-CONSTELLATION was ϵ Lupi.
 459 This system is the only known doubly magnetic massive binary (Shultz et al. [57]).
 460 Pablo et al. [58] were able to determine masses and radii despite an orbital inclination

461 of $\approx 20^\circ$. This allows one to explore the interesting interplay between magnetism and
 462 tidal effects in the evolution of such a system.

463 The value of BRITE heartbeat stars also extends to the upper reaches of the HR
 464 diagram with the enigmatic and highly eccentric binary system η Car, although the
 465 length of the period combined with mass loss have made it difficult to characterize any
 466 heartbeat signal at periastron. Using two separate BRITE observations, Richardson et
 467 al. [59] were able to confirm oscillation frequencies, which appear to be stable over the
 468 past four decades (van Genderen et al. [60], Sterken et al. [61]). These frequencies share
 469 many similarities with TEOs, though this identification will need more data to confirm.

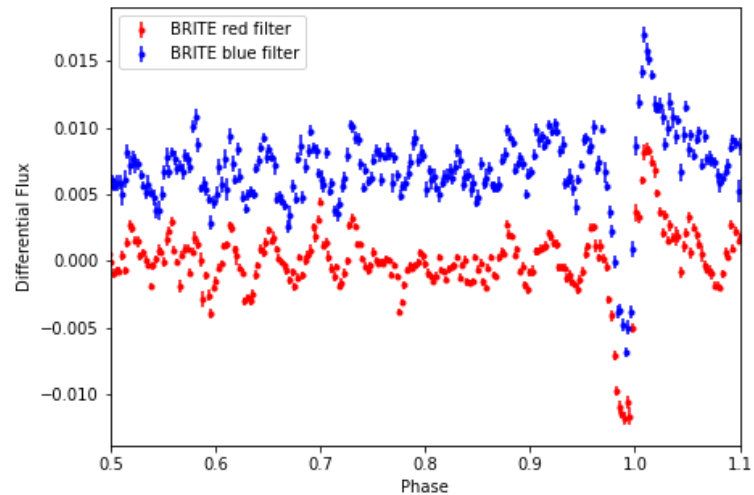


Figure 15. Binned and phased data of ι Ori, obtained with BRITE-CONSTELLATION, covering two years. The data clearly show tidally excited oscillations, most prominently from 0.5 – 0.8 in phase, as well as a strong heartbeat signal (0.95 – 1.05 in phase). The blue points are shifted by a constant flux for clarity.

470 4.3. The riddle of Betelgeuse

471 The red supergiant Betelgeuse is not only one of the biggest stars in the sky, but
 472 also one of the most puzzling. Long-term photometry and radial velocity studies reveal
 473 semi-regular stellar pulsation periods of 420 d, and possibly superposed by a cycle of
 474 8.7 years (Goldberg [62], Dupree et al. [63], Smith et al. [64]). In comparison, Kiss et
 475 al. [65] report 388 ± 30 days as a pulsation period and a 5.6 ± 1.1 years cycle, using
 476 AAVSO-V data obtained almost during an entire century (1918-2006).

477 Curiously, its high apparent brightness makes Betelgeuse a difficult target for
 478 ground-based photometry, as big telescopes suffer from over-exposure. This gap is now
 479 filled with high-quality BRITE photometry (Fig. 16), augmented with spectroscopic data
 480 obtained during more than 10 years at the STELLA robotic observatory, which is one of
 481 the biggest fully robotic telescopes worldwide (Strassmeier et al. [66]). Only automated
 482 observing procedures allow scheduling of almost daily visits of the same star, each
 483 lasting no longer than 5 minutes and stretching over more than a decade. More than
 484 2000 individual, high-resolution spectra have been collected and automatically reduced.

485 As Fig. 16 illustrates, the radial velocity variations follow in general closely the
 486 photometry, suggesting a physical link between photometric and radial velocity vari-
 487 ations. Only during the grand dimming event in the 2020/21 season is an excursion
 488 seen. The photometric amplitude by far outstretches the already high RV amplitude. An
 489 analysis of HST UV-data of this period (Dupree et al. [67]) hints to a big plume of dust
 490 being emitted from the surface of the star and subsequently drifting into the line of sight,
 491 thereby enhancing the photometric minimum.

492 Betelgeuse is approaching its end of life as a star, commonly believed to be a
 493 supernova progenitor. Last year's dimming event sparked estimates that an explosion

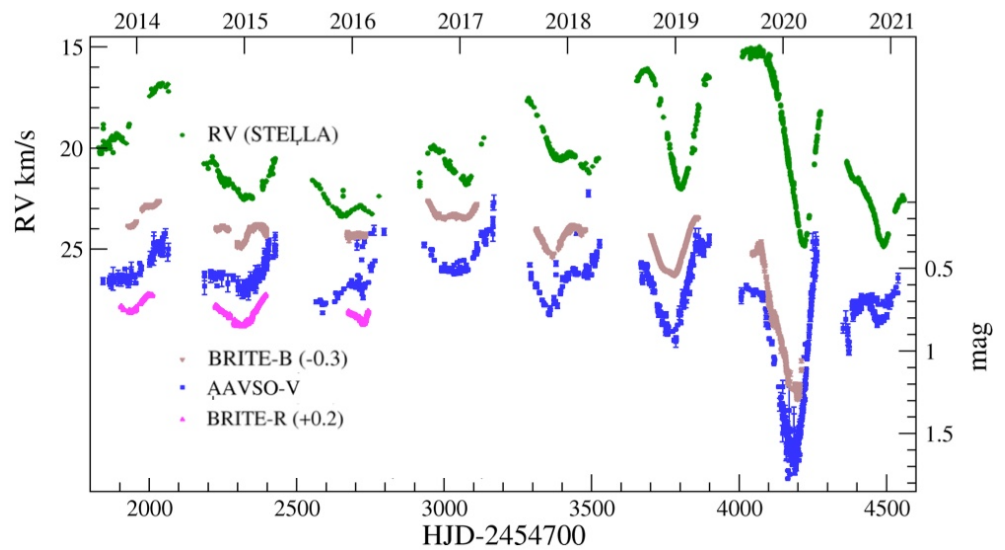


Figure 16. Comparison of light and RV variations of Betelgeuse. From top to bottom: STELLA RV data, BRITE-blue, AAVSO-V absolute photometry, and BRITE-red photometry. Error bars on BRITE magnitudes and on STELLA RV are too small to be visible.

494 may be imminent within the next 100 000 years. But observations and models are
 495 currently not refined enough to prove whether Betelgeuse will end in a type IIb, II-L,
 496 or II-P supernova (Meynet et al. [68]). Hence, new observations are needed to better
 497 estimate mass and rotation rate in order to pin down Betelgeuse’s future path. BRITE-
 498 CONSTELLATION will participate in these campaigns.

499 4.4. Evolving pulsation of the slowly rotating magnetic β Cephei pulsator ζ^1 CMa

500 ζ^1 CMa is a remarkable magnetic early B-type star that is distinguished in several
 501 ways: it rotates extremely slowly ($P_{\text{rot}} \sim 30$ y; Shultz et al. [69]), it is the only magnetic
 502 B-star known to exhibit detectable H α emission from a dynamical magnetosphere ([69]),
 503 and its optical and X-ray magnetospheric emission are modulated according to its ~ 0.2 d
 504 radial pulsation period (Shultz et al. [69], Oskinova et al. [70]).

505 Building on work by Pigulski [71], Jerzykiewicz [72] and Shultz et al. [69], BRITE-
 506 CONSTELLATION photometry (BLb, BHr, BTr) of ζ^1 CMa was employed by Wade et al.
 507 [73], as one of the most recent anchor points to monitor the evolution of its pulsation
 508 period. Combining over one century of photometric and radial velocity monitoring, they
 509 concluded that the period evolution of ζ^1 CMa consists of a secular period lengthening
 510 of roughly 0.3 s/century that can be satisfactorily understood as a consequence of
 511 expansion due to stellar evolution. An additional period evolution - more rapid and
 512 of lower amplitude - remains unexplained, and the authors speculate that it may be a
 513 consequence of rotational modulation or evolution that is restricted to relatively rapid,
 514 short-term episodes, rather than uniform long-term changes. Binariness can be ruled out,
 515 because the corresponding RV variations would have been easily detected.

516 4.5. The triple system β Centauri

517 Massive stars, with initial masses greater than $8 M_{\odot}$, are among the least understood,
 518 but they are extremely important, because they produce the majority of heavy elements.
 519 A fascinating BRITE-Constellation target is the triple system β Centauri (Fig. 17) – also
 520 named Agena – consisting of a massive binary (β Cen AaAb: B1 II and B1 III) with an
 521 eccentric orbit and a more distant and 3 mag fainter companion, also of B-type (Pigulski
 522 et al. [74]).

523 β Cen B was discovered in 2011 as a magnetic star (Alecian et al. [75]). With 17
 524 detected p and g modes, the close massive binary system becomes one of about a dozen

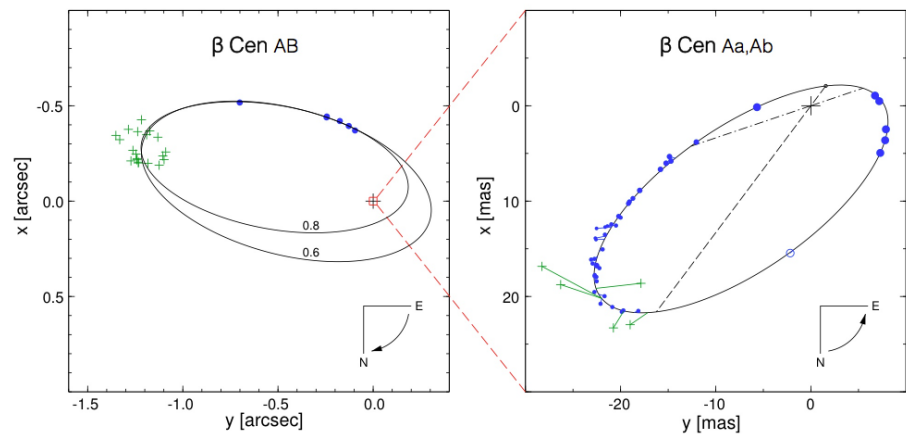


Figure 17. The triple system β Centauri, with two example orbits (eccentricity of 0.6 and 0.8). Adapted from figures 1 and 2 of Pigulski et al. [74].

525 known hybrid β Cep/SPB stars with such a rich frequency spectrum. Furthermore, its
 526 binarity provides a very precise determination of the masses of the components, but
 527 complicates seismic modeling, because the modes need to be safely assigned to one of
 528 the components, which – in addition – are relatively fast rotating.

529 The case of β Cen illustrates the potential of BRITTE-CONSTELLATION data for the
 530 detection of rich-frequency spectra of small-amplitude modes in pulsating stars.

531 4.6. Long-period oscillations in the β Cephei pulsators ν Eridani and θ Ophiuchi

532 Thanks to the long-term stability of BRITTE, Handler et al. [76]) detected several
 533 previously unknown long-period signals corresponding to gravity-mode oscillations of
 534 the β Cephei pulsator ν Eridani. Daszyńska-Daszkiewicz et al. [77,78] demonstrated
 535 that present standard pulsation models cannot reproduce the observed frequency range
 536 of g-mode pulsations, which is likely due to shortcomings in the underlying stellar
 537 physics data, in particular of opacities.

538 Upon the detection of a large number of g-mode pulsations in the BRITTE data of
 539 another β Cephei star, θ Ophiuchi, Walczak et al. [79] arrived at an identical conclusion
 540 (with the caveat that a B5 companion star could be responsible for the g modes), namely
 541 that opacities need to be increased between 30% and 145% (!) in the range $\log T =$
 542 $5.06 - 5.47$ to reproduce the observations. Obviously, the use of correct opacity data is
 543 important for modelling of all kinds of stars. Hence, the implied revision of these data
 544 impacts stellar physics in general.

545 4.7. The ellipsoidal SPB variable π^5 Orionis

546 BRITTE observations of the ellipsoidal variable π^5 Orionis (Jerzykiewicz et al. [80])
 547 revealed that the primary star belongs to the class of Slowly Pulsating B (SPB) stars.
 548 Within the modes of pulsation, there is a re-occurring splitting of twice the orbital
 549 frequency. This is interpreted as perturbation of nonradial pulsation modes by the
 550 equilibrium tide exerted by the companion. The behaviour of the two tidally disturbed
 551 pulsation modes is largely consistent with axisymmetric dipole modes ($l = 1, m = 0$).
 552 These findings have two important and interesting consequences:

- 553 – π^5 Ori is the first SPB star in which tidal perturbations have been identified and
- 554 – these perturbations facilitate the identification of nonradial pulsation modes.

555 BRITTE allowed a valuable proof-of-concept of mode identification to be carried out,
 556 which opened up tidal asteroseismology of SPB stars in multiple systems.

557 4.8. Be stars

558 The BRITE database is rich in Be-star observations because there are many bright
 559 Be stars and, for B-type stars, the blue- and red-sensitive BRITE satellites achieve
 560 roughly equal S/N, unless an extreme reddening is present. The combination of the
 561 frequency resolution and quality of BRITE observations over several seasons with the
 562 long-term behaviour documented by SMEI has achieved qualitatively new insights into
 563 the so-called Be phenomenon.

564 Two central questions about Be stars (see Rivinius et al. [81] for a review) are:
 565 (i) How do Be stars maintain their Keplerian decretion disks where the eponymous
 566 emission lines form and that, without regular replenishment, dissipate within a year?
 567 (ii) How have Be stars acquired their $\gtrsim 75\%$ critical rotation? One way to explain
 568 the latter is mass transfer in a close binary. The former primaries often appear as hot,
 569 subluminal sdO stars that are challenging to detect even in UV spectra (Wang et al.
 570 [82]) and contribute little flux in the BRITE passbands. However, first photometric
 571 Doppler shifts derived from BRITE and SMEI data spanning 25 years have set an upper
 572 limit of $\sim 1 M_{\odot}$ on the mass of a putative companion of ν Pup (Baade et al. [83]).

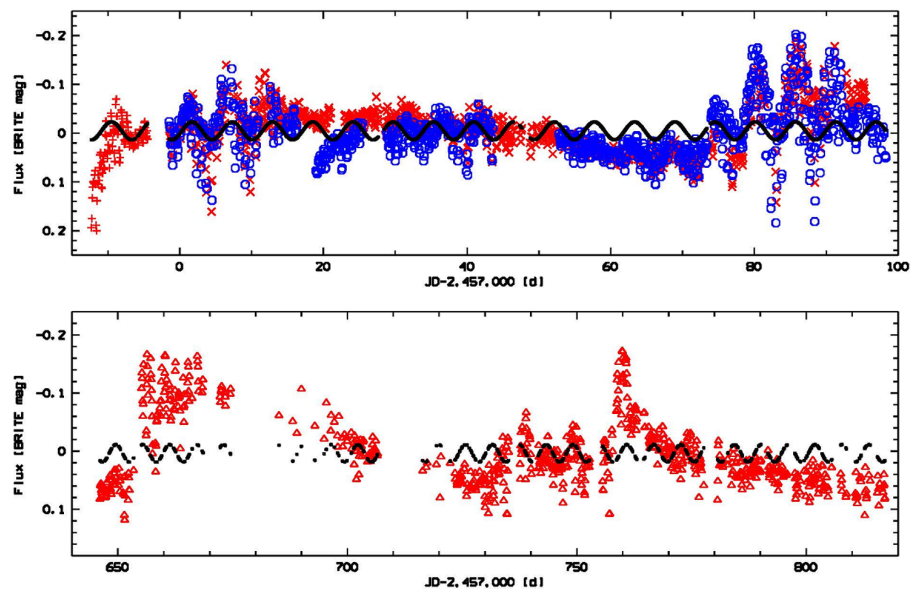


Figure 18. Blue (blue symbols) and red (red symbols) BRITE light curves of the Be star 25 Ori (cf., Baade et al. [89]) from 2014/15 (top) and 2016/17 (bottom). In either season, two outbursts separated by ~ 78 d occurred which corresponds to the difference frequency of 0.0129 c/d between many pairs of non-radial pulsation modes. The black curves are a sine fit to the 2014/15 light curve outside the outbursts with frequency 0.1777 c/d which is another difference frequency in multiple non-radial pulsation frequency pairs. During the outbursts in 2014/15, the light is modulated with 0.1777 c/d, less clearly so in 2016/17. The change in mean magnitude after the outbursts is probably due to increased scattering and free-bound transitions in the subsequently dissipating ejecta.

573 BRITE-CONSTELLATION has been instrumental in confirming earlier suggestions
 574 that Be disks are fed by discrete mass-loss outbursts driven by the superposition of
 575 several low-order non-radial pulsation modes or by recently detected stochastically-
 576 excited pulsations, transporting angular momentum from the stellar core to the surface
 577 (Neiner et al. [84]). Although originally detected in $H\alpha$ line profiles of μ Cen (Rivinius
 578 et al. [85]), optical photometry is a better tracer of outbursts because the V -band flux
 579 responds sensitively to varying amounts of ejecta causing electron scattering and free-
 580 bound recombination (Haubois et al. [86]). In fact, in μ Cen, outbursts have up to
 581 100 times higher amplitude than the underlying non-radial pulsation and can render
 582 the pulsations undetectable (Baade et al. [87]). In η Cen ([87]), 28 Cyg (Baade et al.

583 [88]), and 25 Ori (Baade et al. [89]), BRITE found closely spaced NRP frequencies the
 584 difference between which corresponds to the repeat frequency of the outbursts. During
 585 an outburst, the combined amplitude of the involved non-radial pulsation modes grows
 586 nonlinearly, demonstrating that the outbursts are pulsation powered far beyond mere
 587 mode beating. Hierarchically nested frequency groups can drive repetitive outbursts on
 588 timescales from weeks to years (Fig. 18), and the frequency groups typical of Be stars can
 589 be understood as difference frequencies (g0), non-radial pulsation frequencies proper
 590 (g1), and sum/harmonic frequencies (g2) ([89]). So-called Štefl frequencies first found
 591 in emission lines (Štefl et al. [90]) probably are orbital frequencies in the innermost
 592 inhomogeneous disk (Baade et al. [87]).

593 For shorter timescales/lower amplitudes, TESS (Labadie-Bartz et al. [91,92]) has
 594 confirmed the correlation between increased non-radial pulsation amplitude and mean
 595 brightness. Similarly tight networks of selected non-radial pulsation frequencies do not
 596 seem to be known from other stars, and the outbursts may enable Be stars to escape an
 597 angular-momentum crisis possibly caused by the contracting core (Baade & Rivinius
 598 [93]). The detection of non-radial pulsation modes by BRITE (Borre et al. [94]) and
 599 TESS (Labadie-Bartz et al. [92]) has also terminated decades-long speculations that the
 600 best-known Be star, γ Cas, shows rotational variability due to a magnetic field (Smith &
 601 Henry [95]).

602 4.9. β Lyrae: a binary with a hidden component?

603 A highlight binary is β Lyrae, which consists of a B6-8II bright giant ($3 M_{\odot}$) and an
 604 invisible, more massive companion ($13 M_{\odot}$) producing the primary eclipses. The bright
 605 giant loses mass to the more massive object at a rate that induces a fast period change of
 606 19 seconds per year. There were no previous studies of the intrinsic variability of the
 607 β Lyrae system available which were credible, sufficiently continuous, and uniform, be-
 608 cause of the day-gaps in ground-based observations, which coincided with the prevalent
 609 time-scales of the intrinsic variability in this 12.9-day orbital-period binary.

610 The BRITE data extending over slightly more than 10 full orbital revolutions of
 611 the binary provided the first usable time series, reaching substantially beyond the
 612 intrinsic time scales and permitting utilisation of tools well developed for studies of
 613 variability of active galactic nuclei and quasars. Analysis of the BRITE time series
 614 shows typically three to five instability events per binary orbit, showing a slightly
 615 stronger serial correlation than the red noise (Rucinski et al. [96,97]). The two-parameter
 616 Damped-Random-Walk (DRW) model of the fluctuations (Kelly et al. [98], Zu et al. [99]),
 617 characterised by the red-noise spectrum at time scales shorter than the de-correlation
 618 time scale τ and white noise at longer time scales, agrees very well with the data.

619 The fluctuations are characterised by the amplitude of the stochastic signal of 1.3 %,
 620 expressed relative to the maximum flux from the binary, while the de-correlation length
 621 of the random disturbances is characterised by a typical value of $\tau = 0.88$ days. The
 622 invisible companion is the most likely source of the instabilities. Unexpectedly, the
 623 time scale of the intrinsic variability - most likely associated with the thermal time scale
 624 of mass-transfer instabilities - appears to follow the same dependence on the mass of
 625 the accreting object as is observed for active galactic nuclei and quasi-stellar objects,
 626 which are five to nine orders of magnitude more massive than the β Lyrae torus-hidden
 627 component.

628 4.10. HD 201433 - a Rosetta-stone SPB star in a multiple system

629 Rotation is a still incompletely understood key process of stellar evolution (Aerts et
 630 al. [100]). If stars locally conserved angular momentum, their cores would spin up and
 631 the surviving compact objects would spin much faster than is actually observed. This
 632 implies that present standard models are incomplete and miss essential processes and
 633 correct timescales. A first step towards solving this problem is to detect how angular
 634 momentum is distributed inside stars, as a function of various parameters including age.

635 Prime candidates for such studies, and more easily understood than B-type stars, are
 636 subgiant and red giant stars, as they convey the rotational history of the earlier stages
 637 of evolution and pulsate with mixed p/g modes that carry information about the deep
 638 stellar interior, as is argued in Kallinger et al. [101] and illustrated in Fig. 19.

639 BRITE-TORONTO observed in 2015 the SPB star HD201433 continuously for 156
 640 days [101]. The peaks in the Fourier spectrum of the BRITE observations turned out
 641 to be broader than expected, which triggered the development of a new Bayesian-
 642 based frequency determination technique with a resolution beyond the formal Rayleigh-
 643 criterion. As a proof, three rotationally split triplets are identified in the nearly half-year
 644 long BRITE-data, with central frequencies and splittings agreeing well with those
 645 extracted from the nearly 8 years of SMEI observations.

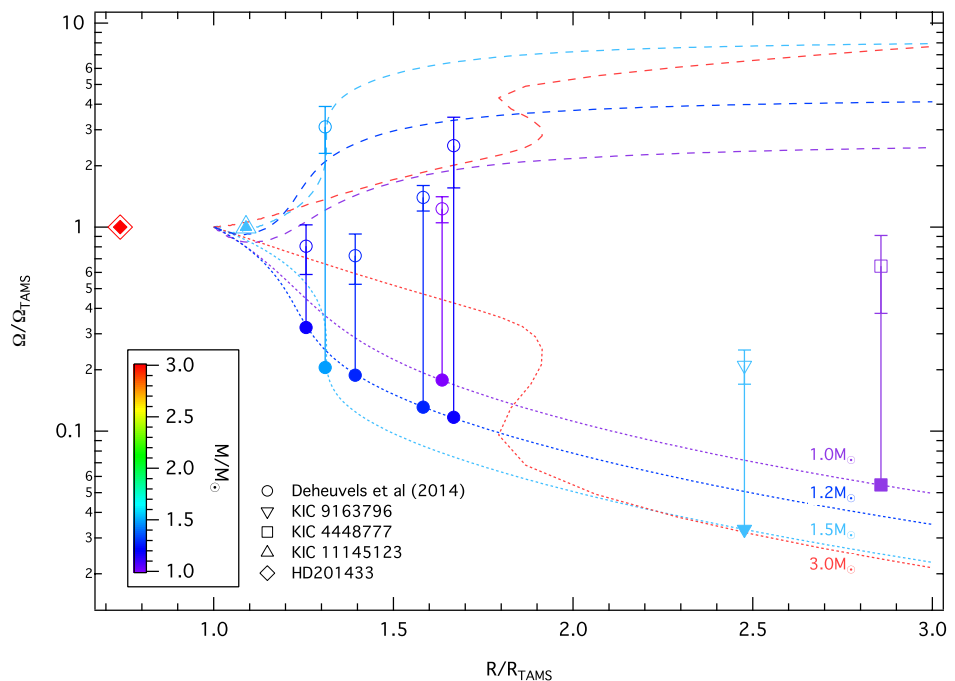


Figure 19. Mean core (dashed lines) and envelope (dotted lines) rotation rate during the evolution of YREC models (from the TAMS to the RGB) with various masses (colour coded) assuming local conservation of angular momentum and rigid rotation on the main sequence. The rotation rate and stellar radius are given relative to their respective values on the TAMS. The filled symbols correspond to the relative envelope rotation rates of various stars with a given mass and radius. The core rotation rate (open symbols) is determined from this value and the observed core-to-envelope rotation gradient (Fig. 19 of Kallinger et al. [101])

646 A science highlight of the HD201433 BRITE-photometry is a trend of splitting
 647 becoming more common towards longer periods, which implies a non-rigid internal
 648 rotation profile, as is elaborated in [101]. For a detailed investigation, a dense grid
 649 of MESA models [102,103] and their non-adiabatic pulsation modes were computed
 650 by Kallinger et al. [101]. Using classical χ^2 techniques and other statistical methods,
 651 a representative model ($3.05 M_{\odot}$ and $2.6 R_{\odot}$) was identified that reproduces best the
 652 observed frequencies.

653 The pulsation modes that are accessible to the seismic analysis probe the radiative
 654 envelope of HD201433 from the boundary of the convective core at about $0.11 R_*$ up
 655 to about $0.98 R_*$. The Bayesian analysis of various rotation profiles provides strong
 656 evidence for a slowly (292 ± 76 d) and rigidly rotating envelope, topped by a thin and
 657 significantly more rapidly rotating surface layer, which covers about the outer 4% of the
 658 radius (Fig. 19). In conclusion, BRITE-CONSTELLATION data provide strong evidence

659 for non-rigid internal rotation in a main-sequence star, which still is rarely presented in
660 the literature.

661 4.11. The young star β Pictoris and its exoplanetary system

662 Exoplanet properties crucially depend on their host star's parameters. The β Pic
663 system includes a wide, dense circumstellar disk that is seen edge-on and two giant
664 gas planets (β Pic b and c) that are only grazingly eclipsing the host star. BRITE-
665 CONSTELLATION data have been used to search for a transiting planet. This puts limits
666 on the β Pic system, as possible planets must be larger than 0.6 (0.75, 1.0) R_{Jupiter} for
667 periods of less than 5 (10, 20) days (Lous et al. [104]).

668 Furthermore, the predicted transit of the Hill sphere of β Pic b triggered an interna-
669 tional observing campaign in 2017-2018 including the BRITE-CONSTELLATION nanosats.
670 No dimming caused by the Hill sphere transit was observed in any of the involved
671 photometric instruments, where the precision of the BRITE photometry would allow
672 detection of a drop in intensity by only 0.5% in the time of interest (Kenworthy et al.
673 [105]). In the spectroscopic observations, some signs of the Hill sphere transit have been
674 detected (e.g., in the Ca II H & K lines) illustrating that the material in the planet's Hill
675 sphere is not sufficiently dense to dim the stellar light enough to be photometrically
676 detected from the ground. In addition, in 1981 anomalous fluctuations of the flux coming
677 from the β Pic system were originally interpreted as being caused by foreground material
678 that transited the stellar disk. Recently, based on the observations conducted within the
679 β Pic Hill sphere transit campaign, Kenworthy et al. [105] showed that this 1981 event
680 did not originate from the transit of a circumplanetary disk.

681 The high-quality BRITE-CONSTELLATION photometry for β Pictoris obtained since
682 2015 provided crucial constraints on the properties of the exoplanet host star itself
683 (Zwintz et al. [106]). The first asteroseismic analysis using multi-color space photometry
684 yielded a precision of 2% in mass and radius for β Pictoris, determined the inclination
685 angle to be 89.1° (which agrees with the inclination angle of the disk of 88.1°), and
686 identified the 15 pulsation frequencies as three $\ell=1$, six $\ell=2$ and six $\ell=3$ p-modes.

687 4.12. The roAp star α Cir

688 α Cir is the brightest rapidly oscillating (roAp) star with a magnetic field. It was
689 discovered in 1981 by Kurtz & Cropper [107] and since then, many publications dealt
690 with photometric and spectroscopic properties, including the magnetic field (see, e.g.,
691 Holdsworth & Brunsden [108] and Weiss et al. [109,110]).

692 α Cir is a text-book illustration for an advantage of nanosatellites dedicated to
693 photometry (e.g. Weiss [19]), as they allow one to observe stars over a long time span.
694 Even if the accuracy of individual data points is inferior to that of larger instruments,
695 long observations of targets result in more accurate frequency spectra. Figure 2 of [110]
696 presents light curves observed by five different satellites with apertures ranging from
697 3 cm (BRITE-blue) to effective 10 cm (TESS) and filter bandwidths of 55 nm and 400 nm,
698 centred on 425 nm and about 800 nm, respectively, (see Table 1 of [110]). The larger
699 the aperture and filter bandwidth, the more accurate the photometry, but if frequency-
700 resolution is important, the picture changes drastically in favour of data obtained over 3
701 years even with a smaller aperture telescope (Fig. 20).

702 Combining the times of maximum from BRITE-red and WIRE data, results in
703 $f_1 = 210.993264(5) \text{ d}^{-1}$, which is, with an error in the corresponding period of 0.01 msec,
704 the most accurately determined dominant pulsation period of any roAp star to date. The
705 main pulsation frequency (f_1) can be identified with an $\ell = 1$ mode, and two additional
706 frequencies likely come from two consecutive radial $\ell = 0$ modes [110].

707 At least three surface spots can be identified for α Cir; the TESS data even suggest
708 a fourth spot. The best-fit (minimum χ^2) set of parameters differs significantly from that
709 inferred from the marginal distributions of the parameters, which hints at a noticeable
710 skewness of the probability distribution of the Bayesian photometric imaging in the

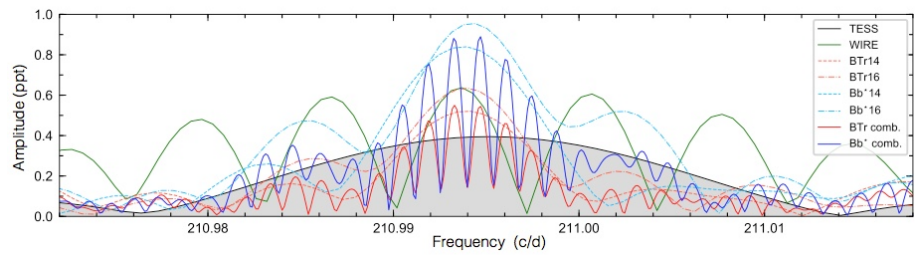


Figure 20. Fourier amplitude spectra of the TESS, WIRE and BRITE photometry, centred on the main pulsation frequency (f_1) of α Cir. BTr14, BTr16, Bb*14, and Bb*16 are the red and blue BRITE data, obtained during the years 2014 and 2016, respectively. Bb* represents the combined blue data obtained with BRITE-Austria and BRITE-Lem. The BRITE-blue amplitudes are divided by two (!) for better comparison with the other data (adapted Fig. 6 of Weiss et al. [110]).

711 considered ten-dimensional configuration space. Obviously, spot latitudes are less
 712 well determined than longitudes, as expected. To our knowledge, this is the first time
 713 that Bayesian-based evidence of models differing in the number of spots has been
 714 quantitatively determined [110].

715 4.13. β Cas: the first δ Scuti pulsator with a dynamo magnetic field

716 One of the cooler BRITE-Constellation targets showing pulsations and a magnetic
 717 field is the F2 type star β Cas, which is also one of the objects in the BRITE legacy fields
 718 (Zwintz et al. [111]). β Cas is a quite unusual star in several aspects:

719 (i) It shows only two independent δ Scuti type p-mode frequencies. As δ Scuti stars are
 720 usually known to show up to hundreds of individual frequencies, this challenges the
 721 asteroseismic interpretation. Why only two frequencies can be detected with a total time
 722 base of over 2.5 years is still unclear.

723 (ii) β Cas is one of the few δ Scuti stars known to date to show a measurable magnetic
 724 field at all [111]. The three other magnetic δ Scuti stars are HD 188774 (Lampens et al.
 725 [112]), ρ Pup (Neiner et al. [113]) and HD 41641 (Thomson-Paressant et al. [114]).

726 (iii) Additionally, the magnetic field structure of β Cas is quite complex and almost
 727 certainly of dynamo origin. One may speculate that the presence of this dynamo field is
 728 related to the unusual lack of numerous δ Scuti frequencies.

729 All this makes β Cas a powerful test bench for modelling of dynamo processes in
 730 thin convective envelopes of F-type stars.

731 4.14. Rotation, pulsation, orbits and eclipses in the constellation of Auriga

732 The Auriga field is an excellent example of an arrangement typically chosen for
 733 observations with BRITE-CONSTELLATION. One or two key targets determine the
 734 orientation of a BRITE satellite and in the same field additional targets with a large
 735 mass-range maximise the science output.

736 Rotation and pulsation periods across the Hertzsprung-Russell diagram are of top
 737 priority for understanding stellar activity as a function of time. Continuous photometry
 738 with up to three BRITE satellites was obtained for 12 targets, primarily in the Aur/Per I
 739 field, and subjected to a period search (Strassmeier et al. [115]). The bright active star,
 740 Capella, was found to be constant in the red bandpass with an rms of just 1 mmag
 741 over 176 d, but showed a 10.1 ± 0.6 d periodicity in the blue, which is interpreted to be
 742 the rotation period of its active and hotter secondary star (Fig. 21). Its position in the
 743 Hertzsprung gap suggests ongoing changes in its internal structure. It is expected that
 744 this has a profound impact on the visible surface and can explain its fast rotation.

745 Results for the other targets in Auriga include:

746 (i) The main pulsation period of the F0 supergiant ϵ Aur is detected by a multi-harmonic
 747 fit of the 152-day long light curve. This is noteworthy, because the RVs observed con-
 748 temporaneously with the Stella spectrograph revealed a clear 68 d period. Although

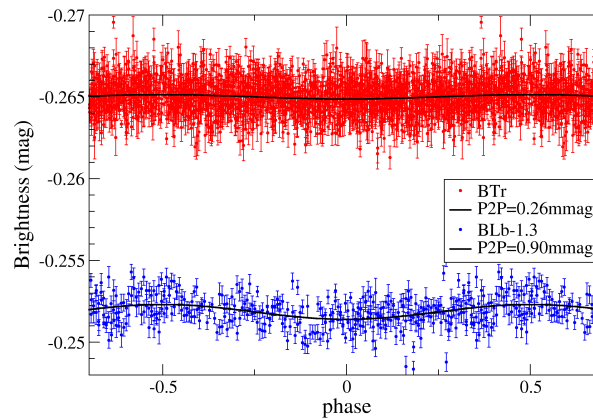


Figure 21. Phase plots for the red (top) and blue data (bottom) with the best-fit 10.1 d period for Capella. The blue data are dominated by the hotter G0 component while the red data are dominated by the cooler G8 component. The rotation period of the cool component is near the orbital period of 104 days (adapted Fig. 3 of Strassmeier et al. [115]).

749 the light curve showed two minima separated by 74 d, a single period of that duration
 750 would not fit the data adequately. These RVs indicated that the (stellar) disk-integrated
 751 pulsations seem to revert when maximum or minimum light is reached, that is, the star
 752 is apparently most contracted when brightest and most expanded when faintest.

753 (ii) An ingress of an eclipse of the ζ Aur binary system was covered and a precise timing
 754 for its eclipse onset derived. We obtained a possible 70 d period from the outside-eclipse
 755 light-curve fits of the proposed tidally-induced, nonradial pulsations of this ellipsoidal
 756 K4 supergiant.

757 (iii) η Aur was identified as an SPB star with a main period of 1.289 ± 0.001 d. Five more
 758 periods are seen in the BRITE photometry and three of these are also seen in the RV
 759 data. The amplitude ratios as well as the phase lags between brightness and RV periods
 760 reflect those expected from low-degree gravity modes of SPB stars. η Aur is thus among
 761 the brightest SPB stars known.

762 (iv) Rotation of the magnetic Ap star θ Aur is easily detected by photometry and spec-
 763 troscopy with a period of 3.6189 ± 0.0001 d and 3.6177 ± 0.0006 d, respectively. The RVs
 764 of this star show a striking non-sinusoidal shape with a large amplitude of 7 km s^{-1} ,
 765 which is likely due to the line-profile deformations from the inhomogeneous surface
 766 distribution of its chemical elements. Such a non-sinusoidal shape likely explains the
 767 small period difference and suggests that the two periods are actually in agreement.

768 (v) Photometric rotation periods are also confirmed for the magnetic Ap star IQ Aur of
 769 2.463 d and for the solar-type star κ^1 Cet of 9.065 d, and also for the B7 HgMn giant β Tau
 770 of 2.74 d. The latter remains uncertain because it was reconstructed only with the very
 771 small amplitude of 0.54 mmag.

772 (vi) Revised orbital solutions are derived for the eclipsing SB2 binary β Aur, which
 773 replaces the initial orbit from 1948, and for the RS CVn binary V711 Tau for which a
 774 spot-corrected orbital solution was achieved. The two K giants ν Aur and ι Aur are found
 775 with long-term trends in both the light curve and the RVs. ν Aur could be a long-period
 776 eccentric SB1 system with a low-mass companion for which a provisional orbital solution
 777 is predicted with a period of 20 yr and an eccentricity of 0.7. The RV variations of the
 778 hybrid giant ι Aur are of even lower amplitude (0.7 km s^{-1}) but shorter period (≈ 4 yrs)
 779 and are more likely due to surface oscillations. Long-term brightness trends were seen
 780 for both stars and appear related with the RVs.

781 4.15. Stellar masses of red giants from their granulation signal

782 A sample of 23 RG stars in the range $1.6 < V < 5.0$ and distributed all over the sky
 783 was investigated by Kallinger et al. [116], and a clear granulation and/or oscillation

784 signal was found. Each star was observed almost continuously by at least one of the five
785 BRITE satellites for up to 173 d.

786 Even though plenty of information is available in the literature for these bright stars,
787 neither surface gravity ($\log g$) nor mass is sufficiently well known. Granulation and/or
788 oscillation timescales, deduced from BRITE-CONSTELLATION observations, help to
789 determine model-independent estimates of $\log g$ with two different methods (Kallinger
790 et al. [117]). Using precise radii from the literature, mostly from interferometric angular
791 diameters and Gaia parallaxes, the mass of the stars can be estimated from $\log g$, derived
792 from BRITE-data, which are dominated by the granulation signal.

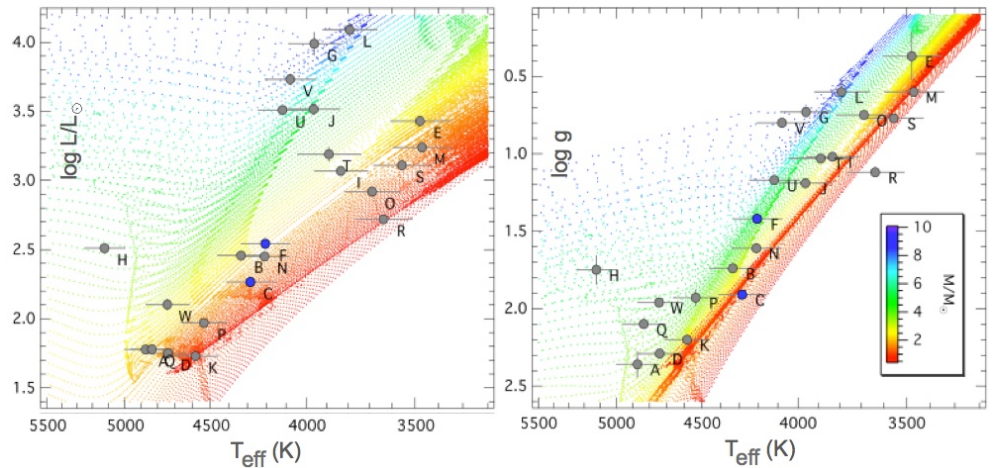


Figure 22. Hertzsprung–Russell diagram (left) and Kiel-diagram (right) with red giants observed by BRITE-CONSTELLATION (grey-filled circles). The small dots show MIST stellar evolution models for solar composition with the mass colour coded. Blue-filled circles mark stars for which solar-type oscillations have been found in the BRITE-CONSTELLATION data (adapted Fig. 10 from Kallinger et al. [116]).

793 The stellar masses presented in Fig. 22 range from about 0.7 to more than $8 M_{\odot}$ and
794 have formal uncertainties of about 10% to 20%, which covers the observational errors
795 as well as the known uncertainties of the used scaling relations. One might question
796 whether simple scaling relations hold for low-mass giants with about $10 M_{\odot}$ to high-mass
797 giants with more than $200 R_{\odot}$, but this is difficult to estimate due to missing independent
798 and reliable mass estimates. Even though there might still be some unknown systematic
799 effects in the scaling relations, they appear to be at least good enough to disentangle
800 low-mass stars from high-mass stars.

801 Comparison of the masses derived through the scaling relations with parameters
802 from a large grid of stellar models also allows one to evaluate statistically the relative
803 evolutionary state of the individual stars i.e., to distinguish low-mass red-clump stars
804 from high-mass red giants.

805 In recent years the seismology of red giants has grown to become an important
806 field in stellar astrophysics, providing the unique opportunity to probe the interior
807 structure of evolved stars (Chaplin & Miglio [118]). In general, seismic scaling relations
808 have become indispensable for determining mass and radius of stars with a convective
809 envelope.

810 4.16. Complete coverage of Nova Carinae 2018 (ASASSN-18fo)

811 This first-time ever observation of a *complete* nova eruption came about by chance.
812 The BRITE-CONSTELLATION had just monitored 18 stars continuously over several
813 weeks in the constellation Carina, when BRITE-Mission-Control (MC, see Sec. 3.2.)
814 recognised a sudden brightening of a field star (inserts in Fig. 23). A quick search
815 among the top sky-news announcements indicated a new star, discovered by the All-Sky
816 Automated Survey for Supernovae (ASASSN) as ASASSN-18fv (Fig. 23).

817 The cooperation of BRITE-CONSTELLATION with the international community is
 818 reported, e.g., in Aydi et al. [120] and resulted in unprecedented simultaneous space
 819 observations in a broad wavelength range and with BRITE starting even before the
 820 actual outburst.

821 A shock model of Metzger et al. [121] predicts that in addition to γ -rays, the
 822 shocked gas should emit mostly in X-rays, which will be absorbed by the dense nova
 823 ejecta ahead of the shocked gas, reprocessed to lower energies, and escape in the optical.
 824 This process indicates a source for the bolometric luminosity of the nova, in addition
 825 to the remnant nuclear burning on the white dwarf surface. Shocks occur in many
 826 transient phenomena, such as Type II supernovae, tidal disruption events, stellar
 827 mergers, superluminous supernovae, etc. Hence, shock interactions may contribute
 828 substantially to the bolometric luminosities of these events, but direct observational
 829 evidence has been lacking. The BRITE-CONSTELLATION observations were unique in
 830 this context and helped to provide insights in many previously poorly observed and
 831 understood phases of novae evolution, see e.g. Hounsell et al. [122], Aydi et al. [123].

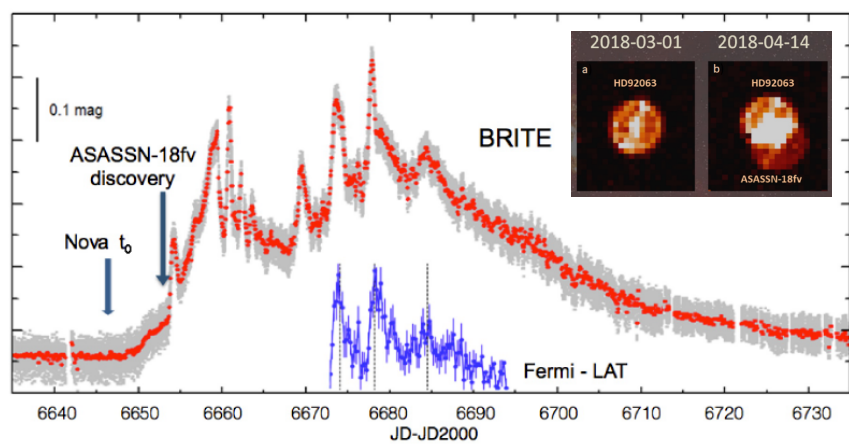


Figure 23. BRITE-TORONTO photometry of Nova Carinae 2018 (grey: individual observations with red filter, red: orbit averages). Blue: Fermi-LAT (Atwood et al. [119]) γ -ray observations. Inserts: raster centred on HD 92063, taken on 2018-03-01 before nova eruption (left), and on 2018-04-14 during nova eruption (right). Scale is 27" per pixel, and exposure times are 4 sec.

832 The well sampled BRITE light curve (Fig. 23) resolves clearly a series of distinct
 833 short-lasting flares of the order of one to two days, but which were poorly resolved from
 834 the ground. γ -rays indicate a series of flares, similar to those in the optical regime, which
 835 suggest:

836 (i) The fact that the flares occur simultaneously in time in both BRITE bands implies
 837 that they very likely share the same origin, i.e. shocks, because they power the γ -rays.
 838 Consequently, shocks are also powering some of the optical emission.

839 (ii) Doubling of the luminosity of the nova during the flares, implies that the shocks
 840 power a substantial fraction of the nova luminosity.

841 (iii) γ -ray and optical light curves (Fig. 23) were very well sampled and indicate a time
 842 lag of approximately 5 hours. This is an additional confirmation that the optical emission
 843 originates in the shocks. γ -rays escape from the shocks with little absorption, but it takes
 844 a few hours to reprocess the X-rays and to emit the energy in the optical regime, exactly
 845 as observed.

846 Fortunately, BRITE-CONSTELLATION observed this nova even before it was discov-
 847 ered, providing “smoking-gun evidence” for the shock model.

848 5. Summary

849 BRITE-CONSTELLATION has outlasted its minimum design-lifetime by several
 850 factors. While it is tempting to terminate the mission, it would be a real pity for humanity

851 to do this, instead of allowing further observations to form a legacy for astronomy. The
852 cost is truly modest compared to most other space missions, especially in relation to the
853 valuable science that BRITE has accomplished and still could accomplish.

854 BRITE-CONSTELLATION's uniqueness lies first in the small sizes of the individual
855 satellites that are capable of three-axis stabilization and providing a pointing stability
856 accurate enough for astrophysical observations. Second, BRITE-CONSTELLATION is
857 an outstanding and unique space mission because of its possibility to observe stars
858 simultaneously in two designated pass-bands and up to 6 months contiguously.

859 The big success of BRITE-CONSTELLATION is reflected - as of March 2021 - in 42
860 peer-reviewed publications and many more conference papers that address a variety of
861 scientific topics from the most massive stars to cool red giants and novae. Here we have
862 highlighted some of the key results as part of a brief overview.

863 **Acknowledgments:** We are grateful to BEST, consisting of two voting members per satellite,
864 supplemented by presently 15 non-voting members, who managed BRITE-CONSTELLATION
865 successfully during nearly a decade. We acknowledge with thanks the variable star observations
866 from the AAVSO International Database contributed by observers worldwide and used in this
867 research. GH thanks the Polish NCN for support (grant 2015/18/A/ST9/00578). AFJM and
868 GAW acknowledge Discovery Grant support from the Natural Sciences and Engineering Research
869 Council (NSERC) of Canada. APo was supported by SUT grant no. 02/140/RGJ21/0012 and
870 Statutory Activities grant no. BK-225/RAU-11/2021

871

- 872 1. http://ntrs.nasa.gov/archive/nasa/casi.ntrs.nasa.gov/19980003950_1997125989.pdf
- 873 2. Code A., Houck T., McNall J., Bless R., Lillie C.: Ultraviolet Photometry from the Orbiting
874 Astronomical Observatory. I. Instrumentation and Operation, 1970, *ApJ* 181, 97
- 875 3. van Duinen R., Aalders J., Wesselius P., et al.: The ultraviolet experiment onboard the
876 Astronomical Netherlands Satellite - ANS, 1975, *A&A* 39, 159
- 877 4. Boggess A., Carr F., Evans D.: The IUE spacecraft and instrumentation, 1978, *Nature* 275,
878 372
- 879 5. Hall D.: The Space Telescope Observatory. Special session of Commission 44, IAU 18th
880 General Assembly, 1982, NASA CP 2244
- 881 6. van Leeuwen F., Evans D., Grenon M., et al.: The Hipparcos mission: photometric data, 1997,
882 *A&A* 323, 61
- 883 7. Kallinger T., Weiss W.: Detecting low amplitude periodicities with Hipparcos, 2002, *A&A*
884 385, 533
- 885 8. Brown A.: The Gaia Mission and its Extension, 2018, IAU Symposium 348
- 886 9. Kuschnig R., Weiss W., Gruber R., Bely P., Jenkner H.: Microvariability survey with the
887 Hubble Space Telescope Fine Guidance Sensors. Exploring the instrumental properties, 1997,
888 *A&A* 328, 544
- 889 10. Kuschnig R., Weiss W. W., Zwintz K.: Microvariability Survey Based on Photometry with the
890 HST Fine Guidance Sensors, 1998, *ASPC* 135, 362
- 891 11. Zwintz K., Kuschnig R., Weiss W. W., Gray R. O., Jenkner H.: Hubble Deep Field guide star
892 photometry, 1999, *A&A* 343, 899
- 893 12. Weiss W. W., Kuschnig R., Zwintz K.: Variability Survey with the HST, 2000, *ASPC*, 203, 38
- 894 13. Zwintz K., Weiss W. W., Kuschnig R., Gruber R., Frandsen S., Gray R., Jenkner H.: Variable
895 HST guide stars, 2000, *A&AS* 145, 481
- 896 14. Kuschnig R., Weiss W., Bahr R.: A Search for Variable Stars based on the HST-FGS Photometry,
897 1996, *swhs.conf.*, 440
- 898 15. Mangeney A., Baglin A., Le Contel J-M., Lemaire Ph., Praderie F., Vauclair G.: Projet de
899 mission spatiale pour l'étude de la variabilité et de l'activité des étoiles: Evris, 1982, proposal
900 to CNES
- 901 16. Vuillemin A., Tynok A., Baglin A., Weiss W. W., Auvergne S., Repin S., Bisnovaty-Kogan G.:
902 Towards Asteroseismology from Space, the Evris experiment. Optomechanical characteris-
903 tics and pointing performances of the Evris/PAIS complex, 1998, *Experimental Astronomy*
904 8, 257

- 905 17. Schneider J., Auvergne M., Baglin A., Michel E., Rouan D., Appourchoux T., Barge P., Deleuil
906 M., Vuillemin A., Catala C., Garrido R., Leger A., Weiss W.: The CoRoT Mission: From
907 Structure of Stars to Origin of Planetary Systems, 1998, ASPC 148, 298
- 908 18. Weiss, W. W., Baglin, A.: High-precision space photometer: CoRoT, 2000, Proc. SPIE 4013,
909 UV, Optical, and IR Space Telescopes and Instruments, 450
- 910 19. Weiss W.W.: Microsatellites, Proceedings of the Vienna Workshop on the Future of Astero-
911 seismology, M. Breger ed., Communications in Asteroseismology 10, 2007, 349
- 912 20. Lemaire P., Appourchoux T., Jones A., Catala C., Catalano S., Frandsen S., Weiss W.: PRISMA:
913 A Space Facility for Studying the Rotation; Interior of Stars, 1992, ASP Conf. Ser. 26, 643
- 914 21. Jones A., Gough D., Andersen B., Baglin A., Bisnovaty-Kogan G., et al.: STARS, Seismic
915 Telescope for Astrophysical Research from Space, 1996, A proposal to ESA for the M3 mission
- 916 22. Favata F., Roxburgh I., Christensen-Dalsgaard J.: Eddington A Mission to Map Stellar
917 Evolution through Oscillations and to Find Habitable Planets, 2000, ESA-SCI(2000)8
- 918 23. Roxburgh I.: Background to the Eddington mission, 2002, Proceedings of First Eddington
919 Workshop, ESASP 485, 11
- 920 24. Plato Science Advisory Team: Plato: Revealing habitable worlds around solar-like stars,
921 2010, ESA-SCI(2010)1
- 922 25. Rucinski S., Carroll K., Matthews J., Stibrany P.: MOST (Microvariability & Oscillation of
923 STars) Canadian Astronomical Micro-Satellite, 2003, AdSpR 31, 371
- 924 26. Borucki W., Koch D., Basri G., Batalha N., Brown T., et al.: Kepler Planet-Detection Mission:
925 Introduction and First Results, 2010, Science 327, 977 - 980
- 926 27. Ricker G., Winn J., Vanderspek R., Latham D., Bakos G., et al.: The Transiting Exoplanet
927 Survey Satellite (TESS), 2014, SPIE Proc. Vol. 9143, 556
- 928 28. Cunha M., Antoci V., Holdsworth D., Kurtz D., Balona, L., et al.: Rotation and pulsation in
929 Ap stars: first light results from TESS sectors 1 and 2, 2019, MNRAS 487, 3523
- 930 29. Antoci V., Cunha M., Bowman D., Murphy S., Kurtz D., (60 more), Weiss, W.: The first view
931 of δ Scuti and γ Doradus stars with the TESS mission, 2019, MNRAS 490, 4040 - 4059
- 932 30. Bowman D.M.: Asteroseismology of high-mass stars: new insights of stellar interiors with
933 space telescopes, 2020, FrASS 7, 70
- 934 31. Burssens S., Simón-Díaz S., Bowman D., Holgado G., Michielsen M., et al.: Variability of OB
935 stars from TESS southern Sectors 1-13 and high-resolution IACOB and OWN spectroscopy,
936 2020, A&A 639, 81
- 937 32. Hacking P., Herter T., Stacey C., Houck J., Shupe D., et al.: The Wide-Field Infrared Explorer
938 (WIRE) Mission, 1997, ASPC 124, 432
- 939 33. Eyles C., Simnett G., Cooke M., Jackson B., Buffington A., et al.: The Solar Mass Ejection
940 Imager (Smei), 2003, Solar Physics 217, 319
- 941 34. BRITE-Link: <https://brite-constellation.at>
- 942 35. Zwintz K. & Kaiser A.: Proceedings of the first BRITE Workshop, 2008, Communications in
943 Asteroseismology, 152, 1
- 944 36. Weiss W., Rucinski S., Moffat A., Schwarzenberg-Czerny A., Koudelka O., et al.: BRITE-
945 CONSTELLATION: nanosatellites for precision photometry of bright stars, 2014, PASP 126,
946 573
- 947 37. Deschamps N., Grant C., Foisy D., Zee R., Moffat A., Weiss W.: BRITE-Constellation, 2009,
948 Acta Astronautica 65, 643
- 949 38. Koudelka O., Unterberger M., Romano P.: Nanosatellites - the BRITE and OPS-SAT missions,
950 2014, e&i Elektrotechnik und Informationstechnik 131, 178
- 951 39. Pablo H., Whittaker G., Popowicz A., Mochacki S., Kuschnig R., et al.: The BRITE-
952 CONSTELLATION nanosatellite mission: testing, commissioning, and operations, 2016, PASP
953 128, 125001
- 954 40. Popowicz A., Pigulski A., Bernacki K., Kuschnig R., Pablo H., et al.: BRITE-CONSTELLATION:
955 data processing and photometry, 2017, A&A 605, A26
- 956 41. Popowicz A.: PSF photometry for BRITE nano-satellite mission, 2018, Proc. SPIE 10698,
957 Space Telescopes and Instrumentation 2018: Optical, Infrared, and Millimeter Wave, 1069820
- 958 42. Zwintz K, Poretti E. eds.: Small satellites - big science, Second BRITE-CONSTELLATION
959 Science Conference, Innsbruck, 2016, Proceedings of the Polish Astronomical Society (PPAS)
960 5, 15
- 961 43. Neiner C., Weiss W., Baade D., Griffin E., Lovekin C., Moffat A.: Stars and Their Variability.
962 Observed from Space, Celebrating the 5th Anniversary of BRITE-CONSTELLATION, 2019,
963 <https://starsandspace.univie.ac.at/home/proceeding/>

- 964 44. Zwintz K., Van Reeth T., Tkachenko A., Gössl S., Pigulski A.: Constraining the near-core
965 rotation of the γ Doradus star 43 Cygni using BRITE-CONSTELLATION data, 2017, *A&A* 608,
966 103
- 967 45. Popowicz A.: Analysis of Dark Current in BRITE Nanostellite CCD Sensors, 2018, Proc. SPIE
968 10698, MDPI Sensors 2018, 18, 479.
- 969 46. Popowicz A., Farah A.: Metastable Dark Current in BRITE Nano-Satellite Image Sensor,
970 2020, MDPI Remote Sens. 2020, 12, 3633.
- 971 47. Ramiaramanantsoa T., Moffat A., Harmon R., Ignace R., St-Louis N., et al.: BRITE-
972 Constellation high-precision time-dependent photometry of the early-O-type supergiant
973 ζ Pupis unveils the photospheric drivers of its small- and large-scale wind structures, 2018,
974 *MNRAS* 473, 5532
- 975 48. Bowman D., Bursdens S., Pedersen M., Johnston C., Aerts C., et al.: Low-frequency gravity
976 waves in blue supergiants revealed by high-precision space photometry, 2019, *NatAs* 3, 760
- 977 49. Nichols J., Huenemoerder D., Naze Y., Lauer J., Ignace R., Miller N.: The zeta Pup Consortium:
978 Correlated X-ray and optical variability in the O-type supergiant ζ Pup, 2021, *ApJ* 906, 89
- 979 50. Lenoir-Craig G., St-Louis N., Moffat A., Ramiaramanantsoa T., Pablo H.: Variability of
980 Wolf-Rayet Stars through MOST(LY) BRITE Eyes, 2020, svos.conf. 191
- 981 51. Chené A., St-Louis N., Moffat A., Schnurr O., Crowther P., et al.; BinaMlcS Collaboration:
982 Investigating the origin of the spectral line profiles of the Hot Wolf-Rayet Star WR 2, 2019,
983 *MNRAS* 484, 5834
- 984 52. Chené A., St-Louis N., Moffat A., Gayley K.: Clumping in the Winds of Wolf-Rayet Stars,
985 2020, *ApJ* 903, 113
- 986 53. Ramiaramanantsoa T., Ignace R., Moffat A., St-Louis N., Shkolnik E., et al.: The chaotic wind
987 of WR 40 as probed by BRITE, 2019, *MNRAS* 490, 5921
- 988 54. Ramiaramanantsoa T., Ratnasingam R., Shenat T., Moffat A., Rogers T., et al.: A BRITE view
989 on the massive O-type supergiant V973 Scorpii: hints towards internal gravity waves or
990 sub-surface convection zones, 2018, *MNRAS* 480, 972
- 991 55. Richardson N., Russell C., St-Jean L., Moffat A., St-Louis N. et al.: The variability of the
992 BRITE-est Wolf-Rayet binary, γ^2 Velorum-I. Photometric and spectroscopic evidence for
993 colliding winds, 2017, *MNRAS* 471, 2715
- 994 56. Pablo H., Richardson N., Fuller J., Rowe J., Moffat A., Kuschnig R., et al.: The most massive
995 heartbeat: an in-depth analysis of ι Orionis, 2017, *MNRAS* 467, 2494
- 996 57. Shultz M., Wade G., Alecian E., BinaMlcS Collaboration: Detection of magnetic fields in both
997 B-type components of the ϵ Lupi system: a new constraint on the origin of fossil fields?, 2015,
998 *MNRAS* 454, L1
- 999 58. Pablo H., Shultz M., Fuller J., Wade G.A., Paunzen E., Mathis S., et al.: ϵ Lupi: measuring
1000 the heartbeat of a doubly-magnetic massive binary with BRITE-CONSTELLATION, 2019,
1001 *MNRAS* 488, 64
- 1002 59. Richardson N., Pablo H., Sterken Ch., Pigulski A., Koenigsberger C., et al.: BRITE-
1003 CONSTELLATION reveals evidence for pulsations in the enigmatic binary η Carinae, 2018,
1004 *MNRAS* 475, 5417
- 1005 60. van Genderen A., Sterken C., de Groot M., Stahl O., Andersen J., et al.: A pulsating star
1006 inside η Carinae I. Light variations 1992-1994, 1995, *A&A* 304, 415
- 1007 61. Sterken Ch., de Groot M., van Genderen A.: A pulsating star inside η Carinae. II. The
1008 variability of the pulsation period, 1996, *A&AS* 116, 9
- 1009 62. Goldberg L.: The variability of alpha Orionis, 1984, *PASP* 96, 366.
- 1010 63. Dupree A., Baliunas S., Guinan E., Hartmann L., Nassisopoulos G., Sonneborn G.: Periodic
1011 Photospheric and Chromospheric Modulation in Alpha Orionis (Betelgeuse), 1987, *ApJL* 317,
1012 L85
- 1013 64. Smith M., Patten B., & Goldberg L.: Radial Velocity Variations in Alpha Orionis, Alpha
1014 Scorpii, and Alpha Herculis, 1989, *AJ* 98, 2233
- 1015 65. Kiss L., Szabó G., & Bedding T.: The variability of alpha Orionis, 2006, *MNRAS* 372, 1721
- 1016 66. Strassmeier K., Granzer T., Weber M., Woche M., Andersen M., et al.: The STELLA robotic
1017 observatory, 2004, *AN* 325, 527
- 1018 67. Dupree A., Strassmeier K., Matthews L., Uitenbroek H., Calderwood T., et al.: Spatially
1019 Resolved Ultraviolet Spectroscopy of the Great Dimming of Betelgeuse, 2020, *ApJ* 899, 68
- 1020 68. Meynet G., Haemmerlé L., Ekström S., Georgy C., Groh J., Maeder A.: The past and future
1021 evolution of a star like Betelgeuse, 2013, *EAS Publications Series* 60, 17

- 1022 69. Shultz M., Wade G., Rivinius Th., Neiner C., Henrichs H., et al.: The pulsating magnetosphere
1023 of the extremely slowly rotating magnetic β Cep star ζ^1 CMa, 2017, MNRAS 471, 2286
- 1024 70. Oskinova L., Nazé Y., Todt H., Huenemoerder D., Ignace R., et al.: Discovery of X-ray
1025 pulsations from a massive star, 2014, NatCo 5, 4024
- 1026 71. Pigulski A.: The light-time effect as the cause of period changes in beta Cephei stars. II.
1027 Sigma Scorpii., 1992, A&A 261, 203
- 1028 72. Jerzykiewicz, M.: Long-term period and amplitude variations in β Cephei stars, 1999, NewAR
1029 43, 455
- 1030 73. Wade G., Pigulski A., Begy S., Shultz M., Handler G., et al.: Evolving pulsation of the slowly
1031 rotating magnetic β Cep star ζ^1 CMa, 2020, MNRAS 492, 2762
- 1032 74. Pigulski A., Cugier H., Popowicz A., Kuschnig R., Moffat A., et al.: Massive pulsating stars
1033 observed by BRITe-CONSTELLATION I. The triple system β Centauri (Agena), 2016, A&A,
1034 588, 55
- 1035 75. Alecian E., Kochukhov O., Neiner C., Wade G., de Batz1 B., et al.: First HARPSpol discoveries
1036 of magnetic fields in massive stars, 2011, A&A 536, 6
- 1037 76. Handler G., Rybicka M., Popowicz A., Pigulski A., Kuschnig R., et al.: Combining BRITe
1038 and ground-based photometry for the β Cephei star ν Eri: impact on photometric pulsation
1039 mode identification and detection of several g modes, 2017, MNRAS 464, 2249
- 1040 77. Daszyńska-Daszkiewicz, J., Pamyatnykh A., Walczak P., Colgan J., Fontes C., Kilcrease D.:
1041 Interpretation of the BRITe oscillation data of the hybrid pulsator ν Eridani: a call for the
1042 modification of stellar opacities, 2017, MNRAS 466, 2284
- 1043 78. Daszyńska-Daszkiewicz, J., Walczak P., Pamyatnykh A., Handler G., Pigulski A. and the
1044 BRITe Team: What Have We Learnt About B-Type Main Sequence Pulsators from the BRITe
1045 Data?, 2018, PTA Proceedings 8, 65
- 1046 79. Walczak P., Daszyńska-Daszkiewicz J., Pigulski A., Pamyatnykh A., Moffat A., et al.: Seismic
1047 modelling of early B-type pulsators observed by BRITe – I. θ Ophiuchi, 2019, MNRAS 485,
1048 3544
- 1049 80. Jerzykiewicz M., Pigulski A., Handler G., Moffat A., Popowicz A., et al.: BRITe-
1050 CONSTELLATION photometry of π^5 Orionis, an ellipsoidal SPB variable, 2020, MNRAS 496,
1051 2391
- 1052 81. Rivinius T., Carciofi A., Martayan C.: Classical Be stars. Rapidly rotating B stars with viscous
1053 Keplerian decretion disks, 2013, A&AR 21, 69
- 1054 82. Wang L., Gies D.R., Peters G.J.: Detection of Additional Be+sdO Systems from IUE Spec-
1055 troscopy, 2018, ApJ, 853, 156
- 1056 83. Baade D., Pigulski A., Rivinius Th., Wang L., Martayan, Ch., et al.: Short-term variability
1057 and mass loss in Be stars. IV. Two groups of closely spaced, approximately equidistant
1058 frequencies in three decades of space photometry of ν Puppis (B7-8 IIIe), 2018, A&A, 620,
1059 A145
- 1060 84. Neiner C., Lee U., Mathis S., Saio H., Lovekin C., Augustson K.: Transport of angular
1061 momentum by stochastically excited waves as an explanation for the outburst of the rapidly
1062 rotating Be star HD 49330, 2020, A&A 644, 9
- 1063 85. Rivinius Th., Baade D., Štefl S., Stahl O., Wolf B., et al.: Multiperiodic Line-profile Variability
1064 and a Tentative Ephemeris for Line-Emission Outbursts of the Be Star μ Cen, 1998, ASP Conf.
1065 Ser. 135, 343
- 1066 86. Haubois X., Carciofi A., Rivinius Th., Okazaki A., Bjorkman J.: Dynamical Evolution of
1067 Viscous Disks around Be Stars. I. Photometry, 2012, ApJ 756, 156
- 1068 87. Baade D., Rivinius Th., Pigulski A., Carciofi A., Martayan, Ch., et al.: Short-term variability
1069 and mass loss in Be stars. I. BRITe satellite photometry of η and μ Centauri, 2016, A&A 588,
1070 56
- 1071 88. Baade D., Pigulski A., Rivinius Th., Carciofi A., Panoglou D., et al.: Short-term variability
1072 and mass loss in Be stars. III. BRITe and SMEI satellite photometry of 28 Cygni, 2018, A&A
1073 610 A70
- 1074 89. Baade D., Rivinius Th., Pigulski A., Panoglou D., Carciofi A., et al.: BRITening up the Be
1075 Phenomenon. 3rd BRITe Science Conference. 2018, Proc. Polish Academy of Sciences 8, 69
- 1076 90. Štefl S., Baade D., Rivinius Th., Stahl O., Wolf B., et al.: Circumstellar Quasi-periods Accom-
1077 panying Stellar Periods of Be Stars, 1998, ASP Conf. Ser. 135, 348
- 1078 91. Labadie-Bartz J., Carciofi A., de Amorim T., Rubio A., Luiz A.: Classifying Be star variability
1079 with TESS I: the southern ecliptic, 2020, arXiv:2010.13905

- 1080 92. Labadie-Bartz J., Baade D., Carciofi A., Rubio A., Rivinius Th., et al.: Short-term variability
1081 and mass loss in Be stars - VI. Frequency groups in γ Cas detected by TESS, 2021, MNRAS
1082 502, 242
- 1083 93. Baade D. and Rivinius Th.: The demystification of classical Be stars through space photometry,
1084 2020, in Proc. Stars and their Variability Observed from Space, eds. Neiner C., Weiss W.W.,
1085 Baade D., Griffin R.E., Lovekin C. C., Moffat, A.F.J., p.35
- 1086 94. Borre C., Baade D., Pigulski A., Panoglou D., Weiss A., et al.: Short-term variability and mass
1087 loss in Be stars. V. Space photometry and ground-based spectroscopy of γ Cas, 2020, A&A
1088 635, 140
- 1089 95. Smith M. and Henry G.: Automated photometry of γ Cassiopeiae: the last roundup, 2021,
1090 arXiv:2103.03972
- 1091 96. Rucinski S.M., Pigulski A., Popowicz A., Kuschnig R., Kozłowski S., et al.: Light-curve
1092 instabilities of β Lyrae observed by the BRITTE satellites, 2018, AJ 156, 12
- 1093 97. Rucinski S., Pigulski A., Kuschnig R., Moffat A., Popowicz A., et al.: Photometry of β Lyrae
1094 in 2018 by the BRITTE satellites, 2019, AJ 158, 148
- 1095 98. Kelly B., Bechtold J. & Siemiginowska A.: Are the Variations in Quasar Optical Flux Driven
1096 by Thermal Fluctuations?, 2009, ApJ 698, 895
- 1097 99. Zu Y., Kochanek C., Kozłowski S. & Udalski A.: Is Quasar Optical Variability a Damped
1098 Random Walk?, 2013, ApJ 765, 106
- 1099 100. Aerts C., Mathis St. & Rogers T.: Angular Momentum Transport in Stellar Interiors, 2019,
1100 ARA&A 57, 35
- 1101 101. Kallinger T., Weiss W., Beck P., Pigulski A., Kuschnig R., et al.: Triple system HD201433 with
1102 a SPB star component seen by BRITTE-CONSTELLATION: Pulsation, differential rotation, and
1103 angular momentum transfer, 2017, A&A 603, 13
- 1104 102. Paxton B., Bildsten L., Dotter A., Herwig F., Lesaffre P., Timmes F.: Modules for Experiments
1105 in Stellar Astrophysics (MESA), 2011, ApJS 192, 3
- 1106 103. Paxton B., Cantiello M., Arras P., Bildsten L., Brown E., et al. : Modules for Experiments in
1107 Stellar Astrophysics (MESA): Planets, Oscillations, Rotation, and Massive Stars, 2013, ApJS
1108 208, 4
- 1109 104. Lous M., Weenk E., Kenworthy M., Zwintz K., Kuschnig R.: A search for transiting planets
1110 in the β Pictoris system, 2018, A&A 615, 145
- 1111 105. Kenworthy M., Mellon S., Bailey J., Stuik R., Dorval P., et al.: The β Pictoris b Hill sphere
1112 transit campaign. Paper I: Photometric limits to dust and rings, 2021, A&A 648, 15
- 1113 106. Zwintz K., Reese D., Neiner C., Pigulski A., Kuschnig, R., et al.: Revisiting the pulsational
1114 characteristics of the exoplanet host star β Pictoris, 2019, A&A 678, 28
- 1115 107. Kurtz D. and Cropper M.: The Discovery of 6.8 Minute Oscillations in α Cir, 1981, IBVS 1987
- 1116 108. Holdsworth D. and Brunsten E.: SALT HRS Capabilities for Time Resolved Pulsation
1117 Analysis: A Test with the roAp Star α Circini, 2020, PASP 132, 5001
- 1118 109. Weiss W., Froehlich H., Pigulski A., Popowicz A., Huber D., et al.: The roAp star α Circinus
1119 as seen by BRITTE-CONSTELLATION, 2016, A&A 588, 54
- 1120 110. Weiss, W. W.; Froehlich, H. -E.; Kallinger, T.; Kuschnig, R.; Popowicz, A. et al.: New BRITTE-
1121 CONSTELLATION observations of the roAp star α Cir, 2020, A&A 642, 64
- 1122 111. Zwintz K., Neiner C., Kochukhov O., Ryabchikova T., Pigulski, A. et al.: β Cas: The first
1123 δ Scuti star with a dynamo magnetic field , 2020, A&A 643, 110
- 1124 112. Lampens P., Tkachenko A., Lehmann H., Debosscher J., Aerts C., et al.: Low-frequency
1125 variations of unknown origin in the Kepler δ Scuti star KIC 5988140 = HD 188774, 2013, A&A
1126 549, 104
- 1127 113. Neiner C., Wade G., Sikora J: Discovery of a magnetic field in the δ Scuti F2m star ρ Pup, 2017,
1128 MNRAS 468, 46
- 1129 114. Thomson-Paressant K., Neiner C., Zwintz K., Escorza A.: The complex fossil magnetic field
1130 of the δ Scuti star HD 41641, 2021, MNRAS 500, 1992
- 1131 115. Strassmeier K., Granzer T., Weber M., Kuschnig R., Pigulski A., et al.: BRITTE photometry
1132 and STELLA spectroscopy of bright stars in Auriga: Rotation, pulsation, orbits, and eclipses,
1133 2020, A&A 644, 104
- 1134 116. Kallinger T., Beck P., Hekker S., Huber D., Kuschnig R. et al.: Stellar masses from granulation
1135 and oscillations of 23 bright red giants observed by BRITTE-CONSTELLATION, 2019, A&A
1136 624, 35
- 1137 117. Kallinger T., Hekker S., Garcia R., Huber D. Matthews J.: Precise stellar surface gravities
1138 from the time scales of convectively driven brightness variations, 2016, SciA 2, 1

-
- 1139 118. Chaplin W. and Miglio A.: Asteroseismology of Solar-Type and Red-Giant Stars, 2013,
1140 ARA&A 51, 353
- 1141 119. Atwood W., Abdo A., Ackermann M., Anderson B., Axelsson M., et al.: The Large Area
1142 Telescope on the Fermi Gamma-ray Space Telescope Mission, 2009, ApJ 697, 1071
- 1143 120. Aydi E., Sokolovsky K., Chomiuk L., Steinberg E., Li K., et al.: Direct evidence for shock-
1144 powered optical emission in a nova, 2020, NatAs 4, 776
- 1145 121. Metzger B., Hascoët R., Vurm I., Beloborodov A., Chomiuk L., et al.: Shocks in nova outflows
1146 - I. Thermal emission, 2014, MNRAS 442, 713
- 1147 122. Hounsell R., Darnley M., Bode M., Harman D., Surina F., et al.: Nova Light Curves From The
1148 Solar Mass Ejection Imager (SMEI) - II. The extended catalog, 2016, ApJ 820, 104
- 1149 123. Aydi E., Chomiuk L., Izzo L., Harvey E., Leahy-McGregor J., et al.: Early Spectral Evolution
1150 of Classical Novae: Consistent Evidence for Multiple Distinct Outflows, 2020, ApJ 905, 62